crystals

MDPI

Article

Evaluation of Processing Parameters in the Solvothermal Synthesis of Cu-Rich Tetrahedrites for Potential Application as Thermoelectric Materials

Itzel J. Soní-Castro [1], Ana B. López-Oyama [2,3,*], Eugenio Rodríguez González [1,*], Deyanira Del Ángel-López [1], Miguel A. Aguilar-Frutis [4] and Juan J. Reyes-Valdez [1]

[1] Instituto Politécnico Nacional, Centro de Investigación en Ciencia Aplicada y Tecnología Avanzada Unidad Altamira, Km 14.5 Carr. Puerto Industrial, Altamira 89600, Tamaulipas, Mexico; itzel_soni@hotmail.com (I.J.S.-C.); ddelangel@ipn.mx (D.D.Á.-L.); juan_jesus_reyes@hotmail.com (J.J.R.-V.)
[2] Departamento de Investigación en Física, Universidad de Sonora, Blvd. Rosales y Transversal, Hermosillo 83000, Sonora, Mexico
[3] Conahcyt-Universidad de Sonora, Blvd. Rosales y Transversal, Hermosillo 83000, Sonora, Mexico
[4] Instituto Politécnico Nacional, Calzada Legaria 694, Col Irrigación, Alcaldía Miguel Hidalgo, Ciudad de México 11500, Mexico; maguilarf@ipn.mx
* Correspondence: ablopezoy@conahcyt.mx (A.B.L.-O.); eugenior62@gmail.com (E.R.G.)

Abstract: The major issue associated with thermoelectric performance is the low efficiency of power conversion. The main challenge is achieving a combination of high Seebeck coefficient, high electrical conductivity, and low thermal conductivity for a significantly improved figure of merit (ZT). Developing strategies include the production of tetrahedrites with an intrinsically low thermal conductivity through the solvothermal method, using a low reaction time and processing temperature. Here, we report on the preparation of Cu-rich tetrahedrites through the solvothermal technique at low temperature, providing a promising strategy for the preparation of materials with potential applications in thermoelectricity. The influence of synthesis reaction time and temperature on the morphological, structural, and thermoelectrical properties of the samples was investigated through different characterization techniques. Tetrahedrite synthesized at 180 °C for 19 h yielded a favorable ZT value of >0.43 and a thermal conductivity of 0.2 Wm^{-1} K^{-1} (423 K), related to the Sb^{3+}/Sb^{5+} and Cu^{+}/Cu^{2+} ratio, as was observed by XPS. The cubic tetrahedrite phase attributed to the (222) plane was confirmed by XRD and TEM and the intense Raman mode observed at 351 cm^{-1}. SEM images revealed that nanotetrahedral Cu-rich tetrahedrites efficiently assemble into spherical structures, resulting in an improvement in the Seebeck coefficient (437 μVK^{-1}) and electrical conductivity.

Keywords: Cu-rich tetrahedrite; solvothermal parameters; thermoelectric efficiency

Citation: Soní-Castro, I.J.; López-Oyama, A.B.; González, E.R.; Del Ángel-López, D.; Aguilar-Frutis, M.A.; Reyes-Valdez, J.J. Evaluation of Processing Parameters in the Solvothermal Synthesis of Cu-Rich Tetrahedrites for Potential Application as Thermoelectric Materials. *Crystals* **2024**, *14*, 888. https://doi.org/10.3390/cryst14100888

Academic Editors: Andrey Prokofiev and Omar Chmaissem

Received: 31 August 2024
Revised: 7 October 2024
Accepted: 9 October 2024
Published: 12 October 2024

1. Introduction

An ideal thermoelectric (TE) material should exhibit a high Seebeck coefficient (S), as typically observed in semiconductors; high electrical conductivity (σ); and low thermal conductivity (κ), which comprises two sources, electronic motion (κe) and lattice phonon motion (κl). Combining these features is a challenge for high-performance thermoelectric materials [1,2]. Enhancing the power factor (PF) and reducing thermal conductivity improves the performance of thermoelectric materials. This can be evaluated from the dimensionless figure of merit, ZT. An important property of a TE that displays a high ZT is the maintenance of a low thermal conductivity, associated with a significant number of atoms per unit cell. A complex crystal structure leads to a high probability of phonon dispersion in the lattice and a highly symmetric crystal system [3–5]. Currently, conventional compounds such as bismuth telluride (Bi_2Te_3) and lead chalcogenides such as PbE (E = S, Se, Te) are still considered efficient thermoelectric materials. However, the most significant obstacle to large-scale production is the inherent high toxicity of Pb, Te, Bi, and Se [6–9]. Therefore, the

development of less toxic materials with enhanced TE performance has become important. In recent years, considerable interest has arisen in regard to producing Cu chalcogenide TE materials due to their high efficiency, optimal PF, and low toxicity [10].

Ternary copper–antimony sulfide compounds, such as chalcostibite ($CuSbS_2$), famatinite (Cu_3SbS_4), skinnerite (Cu_3SbS_3), and tetrahedrites ($Cu_{12}Sb_4S_{13}$), belong to the I-V-VI family of p-type semiconductor materials [11]. These are promising thermoelectric materials because the active lone-pair electrons in the Sb^{3+} ions contribute to their exceptionally low thermal conductivity [12]. The chemical composition of tetrahedrites can be expressed as $A_{12}X_4Y_{13}$, where A represents copper (Cu); X denotes a metalloid, in particular, antimony (Sb) or arsenic (As); and Y represents sulfur (S). Tetrahedrite has a cubic crystal structure that exhibits $I\bar{4}3$ m symmetry. Six of the twelve copper atoms are arranged in planar trigonal sites. The remaining copper atoms are distributed in 12 tetrahedral sites. Additionally, these sites are occupied by Sb atoms bonded to three sulfur atoms, resulting in the formation of holes in the structure and lone pairs around each Sb atom. Because of its complicated chemical structure and tight stoichiometry, obtaining a pure phase of tetrahedrite is a major challenge. The synthesis of tetrahedrites has focused on solid-state techniques, but a further thermal treatment is required to produce a more homogeneous material. In addition, the compacted powders are then sintered, resulting in a process that requires a significant amount of energy because of high temperatures and long processing times, which increase the cost-effectiveness of thermoelectric materials [13].

Some authors have reported that appropriate synthesis parameters for the preparation of tetrahedrites have a significant effect on their thermoelectric properties. Lu et al. synthesized high-performance TE materials with a ZT of 0.9 at 723 K from a natural mineral employing the high-energy ball-milling method. The reported data indicate that the low thermal conductivity of the tetrahedrite crystal structure and the small grain size of the pellets are responsible for the high ZT value [11]. Lee et al. reported the thermoelectric properties of skinnerite, Cu_3SbS_3, hot-pressed alloys. Their findings showed an enhanced Seebeck coefficient and PF ranging from 0.58 to 0.61 mW m^{-1} K^{-2} at 623 K, and a thermal conductivity value below 0.78 Wm^{-1} K^{-1}, with a maximum ZT of 0.57 at 623 K [14]. Baláž et al. synthesized tetrahedrites by mechanochemical and plasma sintering. From their findings, it was demonstrated that the production of CuS (covellite), skinnerite, and famatinite was influenced by milling time. Thermoelectric measurements revealed a maximum ZT value of 0.67 at 700 K and were attributed to a relatively high-power factor of 1.07 mW K^{-2} m^{-1} and a low thermal conductivity of 1.112 W m^{-1} K^{-1}. While tetrahedrites produced through high-energy methods demonstrate promising ZT and PF. values, the goal of producing sustainable materials should be achieved through low-energy techniques [15]. Kareem et al. reported a novel hydrothermal method for the synthesis of $Cu_{11}Zn_1Sb_4S_{13}$ (tetrahedrite and zincian) nanoparticles at a low temperature of 185 °C during 6 h and further annealing at 400 °C for 2 h. The structural, morphological, and optical properties of $Cu_{11}Zn_1Sb_4S_{13}$ nanoparticles were studied using the drop-casting method. The characterization and structure of $Cu_{11}Zn_1Sb_4S_{13}$ by XRD powder diffraction provide evidence for a cubic structure [16].

The solvothermal method makes it possible to produce materials such as semiconductors in novel structures and phases, which are difficult to obtain using other methods. Furthermore, the size, shape, and crystallinity of the products can be controlled via the adjustment of the reaction parameters, such as the temperature (about 500 K), reaction time (15–20 h), solvent type, and pressure. The solvothermal method may reduce energy consumption, making it an environmentally friendly choice alternative for materials' synthesis [13]. The solvothermal method allows the use of low temperatures (160 °C) and the production of tetrahedrites in shorter times than other synthesis techniques. Temperature can be used to influence the reaction kinetics, precursor solubility, reactant stability, and solvent chemical composition [17]. Crystallite size, morphology, and material properties are influenced by the processing time, since longer times allow for extensive nucleation and growth [18]. An et al. reported the solvothermal fabrication of high-quality semicon-

ductor famatinite fibers and tetrahedrite nanoflakes with an over-90% reaction efficiency by varying the quantity of $SbCl_3$, and the solution medium reaction temperature is critical in the synthesis of a pure phase. From their findings, XRD patterns demonstrate that by decreasing the reaction temperature to 120 °C, a significant number of mixed-phase compounds were obtained, while by increasing the temperature to 200–250 °C, the products were mainly tetrahedrites. It has been demonstrated through the selection of the appropriate solvent that the famatinite phase (Cu_3SbS_4) can be synthesized in water instead of ethanol. The structures are composed of large quantities of nanofibers with average diameters of 40–60 nm. It is notable that the utilization of ethanol as a reaction media leads to the formation of a tetrahedrite phase ($Cu_{12}Sb_4S_{13}$). The research demonstrates that the reaction media exert a significant influence not only on the phase of the products but also on the morphology of the final products [19]. Lis et al. reported the solvothermal synthesis of tetrahedrites with 1-(2-aminoethyl) piperazine as a solvent to obtain both copper-rich and copper-poor tetrahedrites with nanometric grain sizes ranging from 40 to 300 nm. The structural and thermal properties of the materials were studied as a function of temperature to revisit the phase evolution of the Cu-Sb-S system near the tetrahedrite compounds. Due to the effective tuning of the carrier concentration, the Seebeck coefficient of the investigated materials changes from 150 μVK^{-1} to 400 μVK^{-1} at 300 K. The prepared tetrahedrites' nanocrystalline nature, which has a significant impact on the strong phonon scattering at grain boundaries, results in an ultralow lattice thermal conductivity of approximately 0.25 $Wm^{-1}K^{-1}$ at 300 K. As a consequence of the precisely tuned electronic transport and the ultralow lattice thermal conductivity, the highest ZT parameter of 0.9 was achieved at 596 K for the nominal composition $Cu_{13}Sb_4S_{13}$ [20]. The controlled morphology is of great importance for improving thermoelectric performance and promoting energy savings by operating in a low-energy condition.

This study demonstrates the synthesis of a Cu-rich tetrahedrite phase prepared using a low reaction time and temperature-dependent assisted solvothermal method. We report that variations in synthesis conditions have a significant impact on the occurrence of a variety of secondary phases, including famatinite, chalcostibite, and covellite, and lead to the production of a purer Cu-rich tetrahedrite. Due to their intrinsically low thermal conductivity, Cu-rich tetrahedrites can be successfully utilized in thermoelectrical applications.

2. Materials and Methods

Cu-rich tetrahedrites were synthesized from the commercial reagents CuCl (Sigma Aldrich, St. Louis, MO, USA, ≥99% purified), $SbCl_3$ (Sigma Aldrich, USA ≥99%), and Thiourea (NH_2CSNH_2, Sigma Aldrich, USA, ≥99%).

2.1. Synthesis of Cu-Rich Tetrahedrites

Cooper(I) chloride, antimony (III) chloride, and thiourea were incorporated in a vessel in a proportion of 1.39:1.21:1 based on the literature synthesis [21] and ultrasonicated for 20 min at room temperature in ethanol (40 mL), as a solvent medium. The mixture was then transferred to a polytetrafluoroethylene (PTFE) vessel (50 mL) and sealed in a stainless-steel autoclave and heated in a furnace at three different temperatures, 165 °C, 180 °C, and 200 °C, for 15, 17, and 19 h, respectively, to evaluate the influence of synthesis parameters such as temperature, time, and pressure on the formation of tetrahedrite compounds. The pressure was not measured in this work, but when the temperature and pressure of the solvent are increased above the critical point, it becomes a special supercritical fluid phase. The autoclave was cooled to room temperature in an oven after the heat treatment was completed. The final product was filtered and washed three times with deionized water and ethyl alcohol-deionized water and then dried at 50 °C in an oven, during 48 h, resulting in a dark powder. For more details, see Supplementary Materials Figure S1.

2.2. Structural and Chemical Characterizations

The structural analysis was performed by X-ray diffraction (XRD). A Bruker D8 Advance X-ray diffractometer was used with CuKα radiation (1.5418 Å) with Bragg–Brentano geometry. The X-ray reflections were identified with the comparison of diffraction patterns in the ICDD Powder Diffraction File (PDF) database. The compositional and morphological analysis was performed using a Scios 2 DualBeam by obtaining the X-ray energy-dispersive spectrometry (XEDS) analysis and the Scanning Electron Microscopy (SEM) images, operated with an EDT detector, using Secondary Electron mode with an accelerating voltage of 20 kV. The powdered samples were deposited directly onto the carbon tape for analysis. High-resolution transmission electron microscopy (HRTEM) and selected-area electron diffraction (SAED) were used to observe the Cu-rich tetrahedrites produced at 200 °C for 15 h (JEM-2010, Japan Electronics Co., Ltd. Tokyo, Japan). A LaB_6 thermionic electron gun was used with an acceleration voltage of 200 kV. Each sample was ethanol-diluted and ultrasonically homogenized for 20 min to facilitate dispersion. Fourier-transform infrared spectroscopy with attenuated total reflectance (FTIR-ATR) was used to study the optical properties of the obtained product. All measurements were conducted using a Perkin Elmer, model Spectrum One, with a scanning range from 4000 to 650 cm^{-1} and an accuracy of ± 4 cm^{-1}.

The elemental composition of the compounds was analyzed by X-ray photoelectron spectroscopy (XPS) in a Thermo Scientific K-alpha, in ultrahigh vacuum, using a monochromatic AlKα X-ray source at 1486.6 eV energy. For the thermoelectric characterization, circular pellets of 10 mm in diameter and 0.8 mm in thickness were compressed at 8 MPa for 15 min. The pellets showed ≥95% the theorical density. The electrical conductivity (σ) and Seebeck coefficient (S) of the circular pellets were measured from 303 to 423 K using a Netzsch SBA 458 Nemesis apparatus. The thermal diffusivity was obtained from the same circular pellets via the laser flash method, using a Netzsch LFA 467 HiperFlash instrument from 303 to 423 K. Finally, the figure of merit (ZT) was calculated as follows:

$$ZT = \frac{\sigma S^2}{k}\overline{T} \quad (1)$$

where σ denotes the electrical conductivity; S represents the Seebeck coefficient; and k stands thermal conductivity, calculated from $k = \alpha \cdots c_p \cdots d$. Here, α represents thermal diffusivity, c_p represents specific heat, and d denotes material density.

3. Results

We investigate the influence of both reaction time and temperature parameters in the synthesis of Cu-rich tetrahedrites by the solvothermal method with a view to their potential application in the development of thermoelectric materials. The investigation of Cu-rich compounds is motivated by the interest in developing materials to eventually reduce conventional thermoelectric materials. It is highlighted that the effect of the reaction time leads to an improvement in the figure of merit for Cu-rich tetrahedrites.

3.1. Spectroscopic Analysis

3.1.1. Fourier-Transform Infrared Spectroscopy

Figure 1a–c depict the spectra of Cu-rich tetrahedrites produced at 165, 180, and 200 °C for 15, 17, and 19 h of time reaction. The main reason for this analysis was to reveal the composition of the materials to detect the organic precursors' traces. The compounds produced at 165 °C showed the typical vibrations of the thiourea around 3334, 1518, 1414, 1079, and 694 cm^{-1}, which were attributed to the NH stretching, NH bending, CN asymmetric stretching, CN stretching, and C=S rocking, respectively. As the temperature increased to 180 and then 200 °C, low intense bands were observed, and in some cases, those were absent. The symmetric stretching and bending bands centered at 3334, 1615, and 1518 cm^{-1} were attributed to the -OH groups of the solvent [22] that probably are

trapped inside the porous structure of the Cu-rich compounds, as was observed in the SEM micrographs. The bands centered at 3275, 3174, 3123, 1414, 1397, and 1615 cm^{-1} were attributed to symmetric and asymmetric N-H stretching, C=N stretching, and N-H bending, respectively. However, the vibration of the C=S bond (735 cm^{-1}) of the thiourea was no longer observed. The band centered at 691 cm^{-1} attributed to the C-S bond was observed, indicating that C=S turns into C-S with the temperature rise. The bands located around 1079 and 1067 cm^{-1} were attributed to the formation of $CuSO_4$ ascribed to the S=O bond of the sulfate groups, in agreement with the Raman spectroscopy analysis. The possible evaporation of the sulfur groups could be responsible for the formation of new by-products during the solvothermal process [23,24]. However, as observed in the 750–650 cm^{-1} region, vibrational modes attributed to CuO are not detectable. We hypothesize that a crystalline CuO structure is not completely produced and that the available copper is used to produce tetrahedrite. For further details, please refer Supplementary Materials Figure S2.

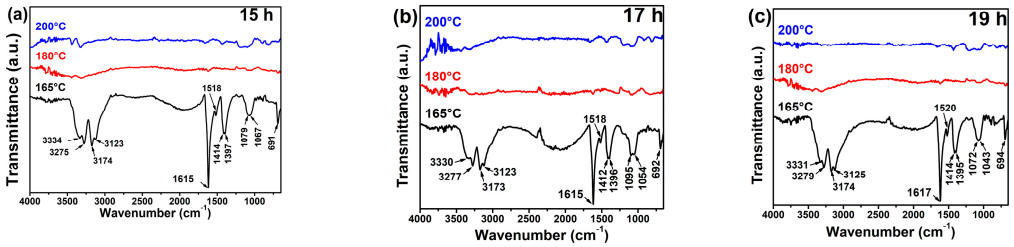

Figure 1. FTIR spectra of the Cu-rich compounds influenced by solvothermal conditions: (**a**) 15 h, (**b**) 17 h, and (**c**) 19 h.

3.1.2. Raman Spectroscopy

The occurrence of possible secondary phases in the solvothermal compounds was investigated using Raman spectroscopy analysis. The micro-Raman spectra of Cu-rich tetrahedrites' compressed powders prepared at 165, 180, and 200 °C during 15, 17, and 19 h are depicted in Figure 2a–i. The Raman spectrum of Cu-rich tetrahedrite powders prepared at 165 °C and 15 h shows modes at 266, 286, 327, 354, and 473 cm^{-1}. The intense Raman mode observed at 354 cm^{-1} is characteristic of the tetrahedrite phase; for more details, see Supplementary Materials Figure S3. The spectra also reveal other less intense peaks located 266 and 286 cm^{-1} that are attributed to vibrations of this phase. Peaks located at 327 cm^{-1} and 473 cm^{-1} are attributed to the Cu_3SbS_4 (famatinite) phase and CuS (covellite) phase, respectively. Powder samples prepared at 165 °C during 17 h show modes at 272, 299, 320, 351, 473, and 490 cm^{-1}. The intense Raman mode observed at 351 cm^{-1} is characteristic of the tetrahedrite phase. The spectra also reveal other less intense peaks located 272 and 299 cm^{-1} that are also lattice vibrations of this phase. The Raman mode observed at 320 cm^{-1} is close to that of the Cu_3SbS_4 (famatinite) phase. According to Prem Kumar et al., the nonappearance of vibration around 323 cm^{-1} is associated with the poor crystalline structure of samples [25]. A mode observed at 473 cm^{-1} is due to the CuS (covellite) phase, in good agreement with Alqahtani et al. [23], and decreases in comparison to samples' growth at 15 h due to the oxidation of Cu, resulting in $CuSO_4$ formation, which can be verified through the shoulder observed at 490 cm^{-1} associated with the $CuSO_4$ phase. Samples prepared at 165 °C and 19 h exhibit modes at 249, 273, 290, 323, 355, and 472 cm^{-1}. At these growth conditions, the tetrahedrite phase was identified through the intense mode observed at 355 cm^{-1}, which appears for all growth conditions. The spectra also reveal other weak modes located at 249, 273, and 290 cm^{-1} that are associated with lattice vibrations of the tetrahedrite phase. Furthermore, the Cu_3SbS_4 (famatinite) and CuS (covellite) phase were identified through the modes observed at 323 and 472 cm^{-1}, respectively. According to the findings, the Sb-S vibration modes of υ1 (symmetric stretching) and υ4 (antisymmetric bending) exhibit the highest-intensity peaks in the 351–357 and 295–300 cm^{-1} regions, respectively. Particularly, the symmetric stretching mode was observed in all solvothermal synthesized compounds

regardless of their growth conditions. The Raman spectra further confirmed the tetrahedrite lattice vibrations assigned to weak broad bands at about 249 cm^{-1} and 266–273 cm^{-1}, respectively. Two vibrational modes, υ2 (symmetric bending mode) at 325–330 cm^{-1} and υ3 (antisymmetric stretching mode) at 345–350 cm^{-1}, were detected in the famatinite phase. In agreement with Rath et al. the $CuSbS_2$ phase of chalcostibite was found at 317 cm^{-1}. Figure 2d–f display the Raman spectra of the compounds produced at 180 °C for 15, 17, and 19 h. The influence of the solvothermal processing conditions plays a key role in the formation of tetrahedrites [24]. Figure 2d shows the Raman spectra of the compounds prepared at 180 °C for 15 h. The lattice vibration modes corresponding to the tetrahedrite phase are not evident under these processing conditions. Chalcostibite and famatinite secondary phases were detected at 317 and 335 cm^{-1}. Furthermore, the intensity of the phase associated with tetrahedrite (355 cm^{-1}) was less intense than that of famatinite. The vibrational mode of the CuS phase is asymmetrical and comprises two internal bands associated with the sulfur modes (464 cm^{-1}) and covellite (479 cm^{-1}) vibrational modes. The compounds produced at 180 °C at 17 h show tetrahedrite lattice vibrations (231, 273, and 298 cm^{-1}), famatinite (326 cm^{-1}), tetrahedrite (352 cm^{-1}), and the covellite phase (471 cm^{-1}) modes, as depicted in Figure 2e. Figure 2f shows the Raman spectra of compounds prepared at 180 °C for 19 h. Interestingly, under these processing conditions, lattice vibrations associated with tetrahedrites (278 and 299 cm^{-1}) are observed. The formation of tetrahedrites may be related to the increase in processing temperature and reaction time, which may lead to a purer phase, since the CuS phase was not observed under these conditions. It is hypothesized that covellite serves as a source of copper atoms for the formation of tetrahedrites. Furthermore, vibrational modes of famatinite (324 and 346 cm^{-1}) are observed. Figure 2g–i show the Raman spectra of the compounds prepared at 200 °C, produced for 15, 17, and 19 h. In addition, Figure 2h shows the Raman spectra of the compounds prepared at 200 °C for 17 h. It is noteworthy that, at 249, 277, and 293 cm^{-1}, the lattice vibrations associated with the tetrahedrite phase are observed. In addition, at 347 and 357 cm^{-1}, respectively, both the famatinite phase and the tetrahedrite phase are observed. We conjecture that an increase in temperature and reaction time may lead to the decomposition of tetrahedrites, as evidenced by the vibrational mode associated with this phase at 474 cm^{-1}. Figure 2i displays the Raman spectra of the compounds produced at 200 °C after 19 h. The disappearance of secondary phases, including chalcostibite, after 19 h (200 °C) results in the formation of famatinite and tetrahedrite compounds, which were identified by their vibrational modes at 324, 347 cm^{-1} (famatinite), and 357 cm^{-1} (tetrahedrite), as well as by SEM micrographs and XRD analysis. Notably, the processing conditions also led to the formation of the covellite phase (474 cm^{-1}). Alqahtani et al. synthesized tetrahedrites and chalcostibite via the decomposition of a mixture of bis(O-ethylxanthate) copper(II) and tris(O-ethylxanthate)antimony(III) and produced a tetrahedrite phase with Cu and Sb atoms in different coordination environments with a cubic structure [23]. The symmetric bending mode at 351 cm^{-1} was associated with the cubic phase of the tetrahedrite, and the absence of this peak in the Raman spectra may indicate poor crystallinity of the sample. The Raman results show the tetrahedrite vibrational mode. At this point, it is important to highlight some trends observed in the results obtained. For a constant reaction temperature (165 °C), and increasing the reaction time, the number of phases present in the sample gradually increases. On the other hand, if the reaction time is constant (19 h), the number of phases in the sample gradually decreases with the increase in the synthesis temperature (200 °C), until finally there are only two phases, in which the tetrahedrite phase is predominant.

Furthermore, our results revealed that by increasing the growing temperature, the signal associated to the covellite phase is reduced and completely vanishes at 200 °C, obtaining a purer sample where only two phases are present (famatinite and tetrahedrite). The copper available in the covellite phase favors the formation of a purer Cu-rich tetrahedrite phase.

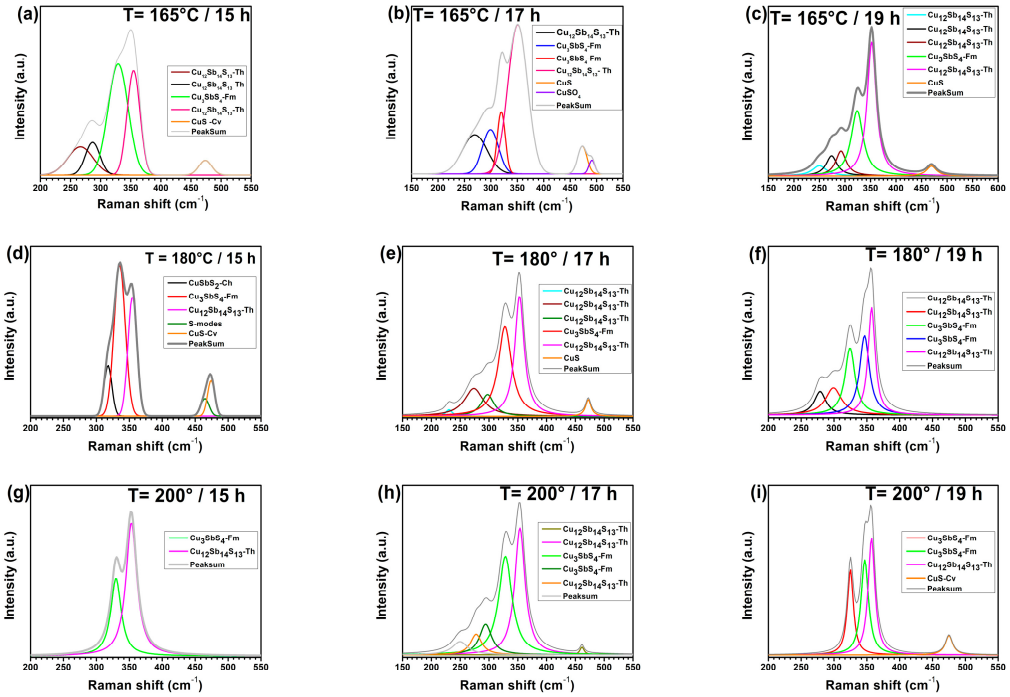

Figure 2. Raman spectra of solvothermal compounds produced with different experimental conditions: (**a**,**d**,**g**) 15 h, (**b**,**e**,**h**) 17 h, and (**c**,**f**,**i**) 19 h.

3.1.3. X-ray Photoelectron Spectroscopy

The X-ray photoelectron spectroscopy (XPS) signals were calibrated using the C 1s peak of the adventitious carbon at 285 eV, and the signals were deconvolved using the Shirley method. Chi-Square values ranged from 0.7 to 2, and for more details, see Supplementary Materials Table S1. XPS measurements provide important information on the oxidation state of Cu in the tetrahedrites. The mono- and divalent contributions of Cu 2p are identified at different energies (BEs) and have distinctly different features, as shown in Figure 3a–i. Pattrick et al. reported that the spectra for divalent Cu are characterized by a narrow single line around 931 eV, whereas monovalent Cu gives a broad peak and an intense satellite at a BE several eV higher [26]. It is well known that Cu has three common oxidation states: Cu^0, Cu^+, and Cu^{2+}, with BE values of 933.7 eV (Cu^{2+}), 932.5 eV (Cu^+), and 932.6/932.7 eV (Cu^0). Other authors have associated the Cu $2p_{3/2}$ peak at 932.98 eV with two shake-up satellites at higher BEs (942.35 and 940.85 eV) [27,28]. The high-resolution XPS (HR-XPS) measurements are depicted in Figure 3a–i and show the typical signals for Cu 2p species, associated with the spin–orbit splitting of the Cu $2p_{3/2}$ and Cu $2p_{1/2}$ core-level peaks. These peaks have a BE of 951.9 and 932.1 eV, respectively. These maximum values show a splitting energy of about 19.8 eV. This value is in good agreement with that reported before [29,30]. The Cu $2p_{3/2}$ and Cu $2p_{1/2}$ core-level peaks are mainly constituted by three inner components in Cu-rich tetrahedrite compounds prepared at 165 and 180 °C, probably related to the different valence states of copper due to the solvothermal process that produces oxidized phases, while the compounds prepared at 200 °C are constituted by two deconvoluted peaks, in good agreement with the formation of a Cu-rich tetrahedrite purer phase. The broader deconvolved peaks at lower BEs of around 932.1 and 951.9 eV are in well agreement with the formation of the Cu^+ state. Besides this valence state, Karikalan et al. attributed these signals to the formation of CuS compounds [31]. In contrast, the species at 933.8 and 953.6 eV are assigned to the Cu^{2+} valence state and low Cu^{2+} surface abundance. The study's evolution of the Cu^+ and Cu^{2+} states' ratio (Cu^{2+}/Cu^+) as a function of the parameter conditions is shown in Table 1.

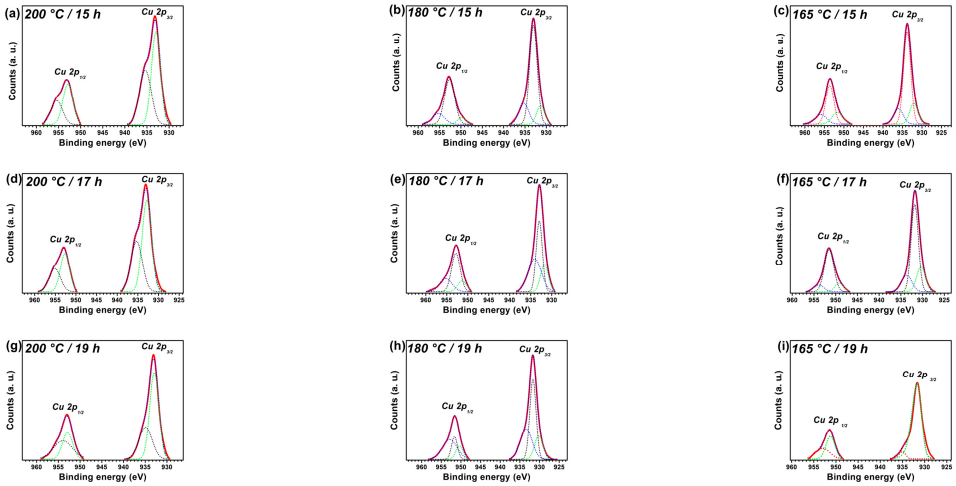

Figure 3. XPS core-level spectra of Cu 2p compounds produced via solvothermal at different processing conditions such temperature and reaction time: (**a**–**c**) 15 h at 165, 180, and 200 °C, (**d**–**f**) 17 h at 165, 180, and 200 °C, (**g**–**i**) and 19 h at 165, 180, and 200 °C.

Table 1. Cu^{2+}/Cu^{+} ratio of the Cu-rich tetrahedrites prepared at different solvothermal conditions.

	Temperature (°C)	Time (h)	Cu^{2+}/Cu^{+} Ratio
Solvothermal conditions	165	15	4.56
		17	3.52
		19	11.23
	180	15	5.32
		17	2.67
		19	3.297
	200	15	—
		17	—
		19	—

From the XPS analysis of Cu-rich tetrahedrites produced at 200 °C, we report two states of copper, Cu^{0} and Cu^{2+}, resulting from the deconvoluted Cu 2p peak. These states can be related to the formation of two compounds, Cu_3SbS_4 (famatinite) and $Cu_{12}Sb_4S_{13}$ (tetrahedrite), as proposed by Wang et al. [28].

According to our results, it can be argued that the only compound that could work with Cu^{2+} states is the $Cu_{12}Sb_4S_{13}$ pure phase. Due to the influence of the solvothermal conditions, the Cu^{+} peak disappeared in the compounds produced at 200 °C, confirming the production of tetrahedrites. The content of copper, antimony, and sulfur in the powders was confirmed via an elemental analysis. A relationship is observed in the Cu^{2+}/Cu^{+} ratio with the increasing temperature and processing time in the solvothermal method to produce tetrahedrites; the Cu^{2+}/Cu^{+} ratio tends to decrease at 15 and 17 h and increases at 19 h.

The abovementioned observations could be observed in the compound produced at 165 °C and at 180 °C. In the compounds prepared at 200 °C, it was not possible to observe the signal corresponding to Cu^{+}. Thus, it can be said that, under these conditions, the compounds produced are mainly tetrahedrites, which can be confirmed by Raman spectroscopy analysis and SEM images. The breakdown of the CuS bond in the covellite phase provides cupper atoms to form the pure tetrahedrite phase.

Figure 4a,b show the typical HR-XPS spectra of the Sb 3d and S 2p species, respectively, for the sample prepared at 200 °C for 15 h. The Sb $3d_{5/2}$ and Sb $3d_{3/2}$ binding energies are at 529.3 and 538.6 eV respectively, corresponding to Sb^{3+} in Cu-rich compounds [32]. See Supplementary Materials Figure S4. We reported a separation energy around 9.4 eV, which is in good agreement with that reported by Vinayakumar et al. [33]. Supplementary Figure

S5 depicts the Sb^{3+}/Sb^{5+} ratio. Figure 4c,d show the signals for S $2p_{3/2}$ at 161.2 eV and S $2p_{1/2}$ at 162.6 eV with a separation BE of 1.2 eV. The peak at 532.0 eV is consistent with adsorbed oxygen. The binding energies for S $2p_{3/2}$ and S $2p_{1/2}$ are 161.9 eV and 163.1 eV, respectively. They are related to the S^{2-} present in $CuSbS_2$. Doublets with higher binding energies of 163.4 eV (S $2p_{3/2}$) and 164.6 eV (S $2p_{1/2}$) have been attributed to a small amount of surface CuS, as indicated by Wan et al. [34].

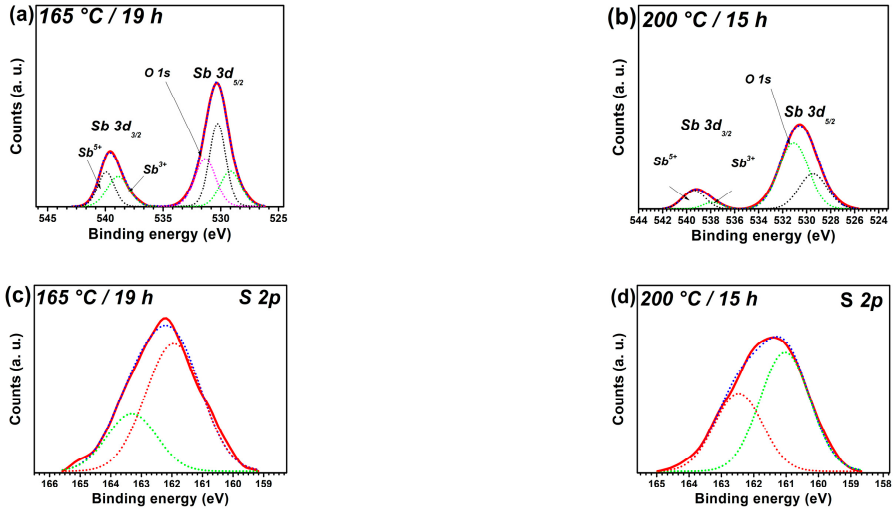

Figure 4. High-resolution XPS spectra for the core level of Sb 3d of the compounds produced at two different temperatures and reaction times: (**a**) 165 °C at 19 h and (**b**) 200 °C at 15 h. Additionally, the S 2p spectra of the compounds produced at (**c**) 165 °C for 19 h and (**d**) 200 °C for 15 h.

In conclusion, the valence of Cu, Sb, and S of the samples synthesized at 180–200 °C is consistent with tetrahedrite formation after 15 h, together with some unreacted binary phases. Such phases were observed to remain on the powders at the end of the process, according to the Raman analysis. However, from 180 °C to 200 °C, an increase in the Cu^{2+} state is observed, indicating the presence of two phases of copper–antimony sulfide, also supported by the Raman analysis. In the XPS spectra of Cu-rich tetrahedrites prepared at 200 °C for 15, 17, and 19 h, there is no peak at ca. 199 eV, which is the fingerprint peak of the Cl from CuCl and $SbCl_3$, meaning that, with the increasing temperature and reaction time, the chloride is completely removed from the solvothermal process for the preparation of a purer Cu-rich tetrahedrite phase [35]. Given that under these solvothermal conditions (200 °C), no oxidized phases were detected either in Raman nor FTIR., it is possible to infer that the crystalline phase, such as CuO, does not exist as a pure phase within the Cu-Sb-S system and undergoes partial oxidation at room temperature due to exposure to air, rather than solvothermal-produced tetrahedrites.

3.2. Structural Analysis

X-ray Diffraction Patterns

The crystal structure and phase purity of the tetrahedrites were analyzed by X-ray diffraction. Figure 5a–c show the X-ray diffraction patterns of samples containing Cu, Sb, and S synthesized at 165, 180, and 200 °C for three reaction times of 15, 17, and 19 h each. From a reaction time of 15 h and temperature of 165 °C, four products were identified in the XRD spectra of the analyzed samples, which included covellite CuS (space group: P63/mmc), chalcostibite $CuSbS_2$ (space group: Pnam), famatinite Cu_3SbS_4 (space group: $I-42$ m), and tetrahedrite $Cu_{14}Sb_4S_{13}$ (space group $\overline{I}43$ m). According to the XRD results, the crystalline structures of the samples display important changes due to the synthesis parameters (time and temperature). At each reaction time and temperature, the diffractograms show characteristic signals of the $Cu_{14}Sb_4S_{13}$ tetrahedrite phase. The diffraction peaks in the patterns coincide well with the standard reference file JCPDS

No. 42-056, and the most intense diffraction peaks are located at 2θ = 29.95°, 49.90°, and 59.39°, attributed to the (222), (440), and (622) planes of the tetrahedrite cubic phase, respectively. The diffractograms also show lower intense peaks located at 2θ = 32.4°, 34.7°, 36.9°, 44.7°, and 54.7°, which correspond to the (321), (400), (330), (510), and (622) planes of the cubic tetrahedrite phase, respectively. The diffractograms also display the typical signals of the chalcostibite ($CuSbS_2$) phase at 2θ = 28.42°, 28.72°, 42°, and 52°, assigned to the (111), (410), (321), and (212) planes of the orthorhombic phase, respectively. The positions of the peaks agree well with those reported for this phase in JCPDS card No. 44-1417.

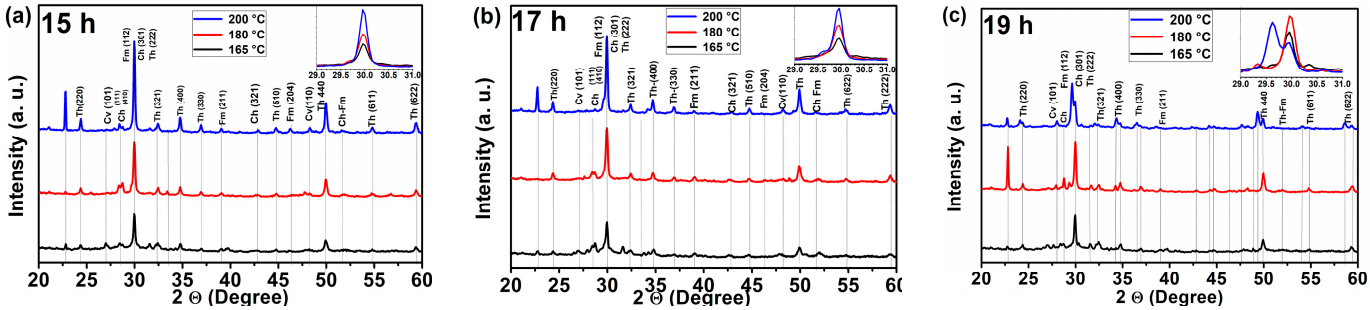

Figure 5. Powder XRD patterns of different compositional Cu-rich tetrahedrites produced during (**a**) 15h, (**b**) 17h, and (**c**) 19 h at 165, 180, and 200 °C. The inset shows the 29° < 2θ < 31° interval.

The most intense signals (100% intensity) for the three most abundant phases found in the samples are located at 2θ = 29.053° (famatinite, (112)), 2θ = 29.910° (chalcostibite, (301)), and 2θ = 29.95° (tetrahedrite, (222)). Consequently, a significant overlap of the corresponding signals around 2θ = 29.5° was observed, and therefore it may be challenging to identify which of the two phases is present from the diffractograms. Bincy et al. synthesized chalcogenide nanoparticles at a range of temperatures between 200 °C and 240 °C. They found that, as the temperature increases, significant changes take place in the crystal structure, optical properties, and electrical performance of the material. They demonstrate that temperature is responsible for the formation of pure Cu_3SbS_4 to $CuSbS_2$ nanoparticles for photovoltaic applications [36].

In this work, we report that, as the temperature increases, the intensity of the diffraction signals increases, the peak FWHM decreases, and, consequently, the crystallite size increases. Temperature influence has a significant impact on the formation of purer tetrahedrite phases. When the temperature is set to 165 °C, a high content of phase mixtures of Cu-rich compounds is observed. Furthermore, we found that famatinite, chalcostibite, covellite, and tetrahedrite subphases were also produced. The cubic tetrahedrite phase was successfully produced at each reaction time and temperature. However, a greater amount of tetrahedrite structures was observed from 180 to 200 °C. The signals associated with the chalcostibite phase (around 28°) decrease as the synthesis temperature increases, while the signal associated with the tetrahedrite increases with the increasing temperature. An et al. reported that both hydrothermal and solvothermal methods are appropriate for the synthesis of famatinite nanofibers and tetrahedrite nanoflakes. The role of the reaction temperature in controlling the phases and morphology of the resulting products was found to be significant [19]. It is important to emphasize that the reaction time has an important effect on tetrahedrite formation, but the optimal time and temperature conditions for obtaining tetrahedrites in their pure phase was from 180 to 200 °C at 19 h. All peaks in the pattern for the tetrahedrites could be indexed to a cubic copper–antimony sulfide with a lattice parameter a of 10.31 Å. Supplementary Materials Figure S6 shows the cell parameters of Cu-rich tetrahedrites synthesized at different processing conditions, such as time and temperature, which is in good agreement with the literature. The peaks for the impurity phases in Figure 5 are much smaller than those for tetrahedrite.

3.3. Morphological Analysis

3.3.1. Scanning Electron Microscopy

Scanning electron microscope (SEM) images of samples synthesized under different processing conditions are shown in Figure 6a–i. At 165 °C and the 15 h reaction time, the compounds are mainly formed by micrometric rod-like structures. These appear as bundles, possibly due to the secondary phases including chalcostibite, famatinite, covellite and tetrahedrite, which have also been identified by XRD and Raman spectroscopy. In addition to rods, sparse microspheres with an average diameter around 5–10 microns, formed by well-defined tetrahedral structures characteristic of tetrahedrite, are observed. However, rods predominate. The appearance of a secondary phase consisting of a rod-like structures was previously reported by An et al. They reported rod structures with uniform diameters in the range of 50–60 nm and 3–4 μm in length, attributed to the chalcostibite phase [37]. Our SEM images reveal a small number of fibers coexisting with a significant number of spherical structures, which are also formed by well-defined tetrahedral structures. As the temperature further increases, the highly cohesive rod-like structures tend to separate into fibers like a fringed rope. The fragments released from the elongated fibers appear to be precursors to the formation of tetrahedral structures. From the abovementioned information, it can be concluded that the secondary chalcostibite phase evolves to form more complex structures, such as a tetrahedrite. The XRD and Raman spectroscopy results confirm that the structures are also Cu-rich compounds, such as chalcostibite, covellite, famatinite, and tetrahedrites. The scenario is quite different when the temperature is increased to 200 °C, as SEM images of the sample surface no longer show fibers or rod-like structures; instead, they show platelet fragments of rods coexisting with many sphere-like structures. The rods forming cohesive platelet-like structures appear to have fragmented into smaller structures, such as tetrahedra, which then assemble into layers to form micrometer-sized spherical structures, which in turn are composed of small tetrahedra. The high processing temperature favors the evolution of secondary phases from the Cu-rich compounds to form tetrahedron-like structures, which in turn decompose into smaller structures. The Raman spectroscopy results support the formation of a purer phase in which only the tetrahedrite and famatinite phases coexist. However, XRD shows that the famatinite phase almost disappears and the tetrahedrite phase predominates over the secondary phases. Fasolin et al. reported the preparation of tetrahedrites by the solvothermal method at 200 °C. The authors suggested that the secondary phases and the tetrahedrite phase were produced because of their similar compositions. They identified the secondary phases as micrometer crystals, while the tetrahedrite phase was observed as nanometer grains [38].

We observe differences in the morphology of the tetrahedrites synthesized at 165 °C for 15 and 17 h. The fibrous structures are no longer observed, and the surface contains rods with a more cohesive morphology, and they seem to break into smaller fragments, such as compacted platelets. The rods appear smoother compared to those produced at 15 h, and some structures, such as buds, are visible on their surface. We also noticed highly cohesive structures in the form of platelets and tetrahedral structures in a spherical arrangement. It is evident that the reaction time influences the appearance of structures such as tetrahedrites. When the temperature was increased to 180 °C, the rods almost disappeared, and the samples appeared as spheres consisting of tetrahedral structures. An interesting phenomenon occurs at 200 °C: no rods are observed; instead, the sample surface contains spherical microstructures made up of sub-micron tetrahedral structures, suggesting that the subphases have decomposed, leading to a tetrahedral phase in a significant proportion. At this point, we observe cohesive and compacted structures, but the most abundant phase is undoubtedly the tetrahedrite, which coexists with flower-like structures that are observed to be polydisperse in shape and size. Wang et al. prepared chlorine-doped hierarchical famatinite with a flower-like arrangement by the solvothermal method. The authors reported that CuS flower-like microspheres composed of nanoflakes served as an intermediate for the synthesis of famatinite [39]. This is related to the Raman spectroscopy

analyses where it was found that the CuS acts as self-sacrificing structural templates to guide the reaction until the desired products are formed. In addition, microstructures consisting of tetrahedrons in a spherical arrangement are also observed.

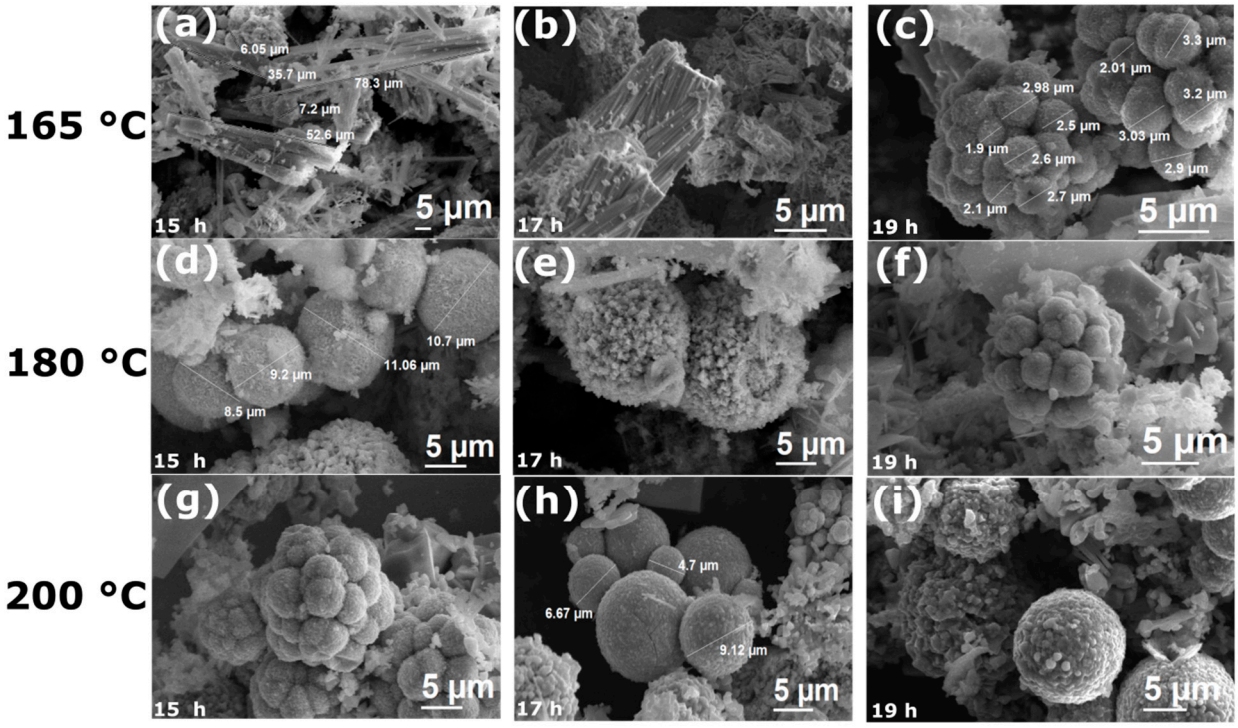

Figure 6. SEM micrographs of the Cu-rich tetrahedrites microstructures prepared via solvothermal method at different processing conditions: (**a**–**c**) at 165 °C during 15, 17, and 19 h; (**d**–**f**) at 180 °C during 15, 17, and 19 h; (**e**–**i**) at 200 °C during 15, 17, and 19 h.

The occurrence of chalcostibite rods in the sample was observed by extending the reaction time up to 19 h, at low temperatures (165 °C). It is important to mention that, under these conditions of processing, it was observed that an increased number of spherical aggregates were arranged in the form of grape bundles, apparently arising from the highly condensed structures, possibly because of the highly cohesive platelet structures. At these processing conditions, the tetrahedrite phase (spheres) exhibits increased dispersity in both shape and size, which may be related to the improved thermoelectric properties. When the temperature is increased to 180 °C, the aggregates remain polydisperse in shape and size. It is observed that highly cohesive and large platelets, over 50 microns in size, tend to break up into nanometer-sized disks. These disks probably play a role in the formation of the tetrahedrons that make up the tetrahedrites from the decomposition of chalcostibite rods. The aggregates produced at low reaction times and high temperatures were not well defined, which may indicate that temperature produces a purer phase of tetrahedrites even with increasing time, according to the results presented in the section covering Raman and diffraction spectroscopy in this report.

It is feasible to form spherical aggregates of tetrahedrites at 200 °C. However, the surface of the tetrahedrons has irregularities, probably due to some structural change responsible for the asymmetric XRD peak typical of tetrahedrites. Lowering the temperature and reaction time results in the formation of smaller and even elongated structures rather than clusters of tetrahedrites. Tetrahedrites undergo fragmentation and possible disintegration in secondary phases, resulting in the formation of highly condensed platelets with aggregate sizes greater than 5 microns. The morphology and size of the tetrahedrites suggest the occurrence of nanometer-sized particles with an estimated average size of 30 nm. Scanning electron microscope (SEM) images reveal that these nanostructures have

a tetrahedral structure, which is consistent with the natural structure of tetrahedrite. It is noteworthy that as the reaction temperature increases, the definition of each nanotetrahedron becomes more defined. This can be seen more clearly in the high-resolution images shown in Figure 6.

Regulacio et al. fabricated tetrahedrites by the solvothermal method from 180 °C to 200 °C for 16 h; they reported the formation of tetrahedral crystals with voids or cavities ranging from 3 to 20 nm in size [40]. Our results show that the effect of temperature and reaction time on tetrahedrite formation results in a purer phase at temperatures ranging from 180 to 200 °C. In addition, longer reaction times and lower temperatures result in more defined tetrahedrites without voids or cavities. SEM micrographs of Cu-rich tetrahedrites synthesized at 165 and 200 °C for 15, 17, and 19 h and their corresponding XEDS are shown in Supplementary Materials Figure S7.

3.3.2. Transmission Electron Microscopy

TEM images of the tetrahedrite $Cu_{14}Sb_4S_{13}$ show the formation of agglomerated particles in the nanometric range (Figure 7a). This agrees with the SEM results. The lattice fringes' spacing was estimated to be 0.291 nm, which corresponds to the (222) lattice plane of cubic tetrahedrite phase. The circular ring pattern of the $Cu_{14}Sb_4S_{13}$ tetrahedrite is shown in the inset of Figure 7a. Diffraction rings correspond to the (220), (211), (220), and (222) family of planes with interplanar spacings of 4.982, 4.197, and 0.291 nm, respectively. These values are in good agreement with those reported in PDF card 00-024-1318 for the cubic tetrahedrite $Cu_{14}Sb_4S_{13}$ and are consistent with the XRD patterns of these materials. Figure 7b shows a HRTEM image of tetrahedrite processed at 180 °C for 15 h. A lattice spacing of 0.355 nm could be measured from the image and was attributed to the (222) plane of the tetrahedrite cubic phase.

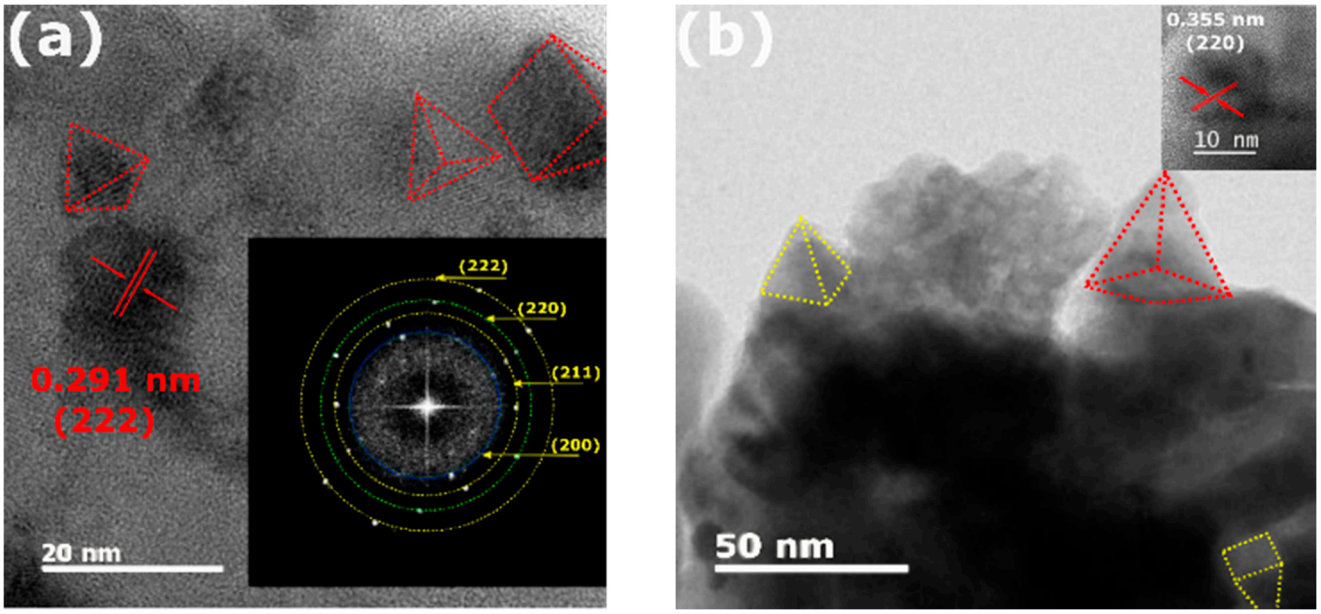

Figure 7. (**a**) HRTEM image of $Cu_{12}Sb_4S_{13}$ displaying lattice spacings of 0.291 nm attributed to the (222) plane of the cubic tetrahedrite. Furthermore, several nanotetrahedral shapes are observed. Inset in (**a**) displays the corresponding circular ring pattern. (**b**) TEM image of tetrahedrites. Red and yellow shapes highlight tetrahedral shapes of nanostructures. The inset in (**b**) shows the lattice spacings of 0.355 nm attributed to the (222) plane of the cubic tetrahedrite.

Selected TEM micrographs and SAED patterns of Cu-rich tetrahedrites are shown in Supplementary Materials Figure S8. An analysis of over 20 HRTEM images revealed that essentially only the cubic tetrahedrite phase grows under these synthesis conditions.

3.4. Thermal Properties of Tetrahedrites

3.4.1. Temperature Dependence of Electrical Conductivity

Figure 8a shows the temperature dependence of the materials fabricated at 15 h. The tetrahedrites prepared at 165 °C show an electric conductivity value of 2.3×10^3 S/m. However, the tetrahedrites produced at 180 °C have a conductivity of 5.1×10^4 S/m, whereas the tetrahedrites produced at 200 °C have an electric conductivity of 2.1×10^3 S/m at 453 K of the temperature range analyzed. For a reaction time of 17 h, the electrical conductivity values for the tetrahedrites prepared at 165, 180, and 200 °C were 1.3×10^3, 2.9×10^3, and 1×10^4 S/m, respectively. At 19 h of reaction time, the electrical conductivity values for the tetrahedrites obtained at 165, 180, and 200 °C were 3.4×10^3, 1.8×10^3, and 2.3×10^3 S/m, respectively. As can be seen from the graphs of the temperature dependence of the electrical conductivity, the tetrahedrites produced at 165 °C, regardless of reaction time, do not exhibit a high electrical conductivity value, while the tetrahedrites produced at 15 h and 180 °C display the highest electrical conductivity (5.14×10^4 S/m). It should be emphasized that the tetrahedrites obtained at 19 h and 180 °C have an electrical conductivity value of 18085 S/m and the highest ZT value (0.43) achieved in this investigation. An increase in the electrical conductivity of a material is attributed to a high concentration of charge carrier that consequently increases the σ values, maybe due to the Cu-rich phases' increase. These results are in good agreement with other TE materials previously studied [41]. Reducing the sulfur-rich compounds leads to an increase in σ, implying the production of a purer phase of the tetrahedrites due to the evolution of secondary phases such as chalcostibite. An increase in the Cu-rich phase provokes the substitution of Sb^{3+} by Cu^{+} and/or Cu^{2+} and possibly increases the charge concentration. The disruption of the current flow by dislocations resulting from the processing method may be responsible for the low electrical conductivity. In our study, the high pressure, reaction time, and processing temperature of solvothermal conditions may have influenced the TE performance.

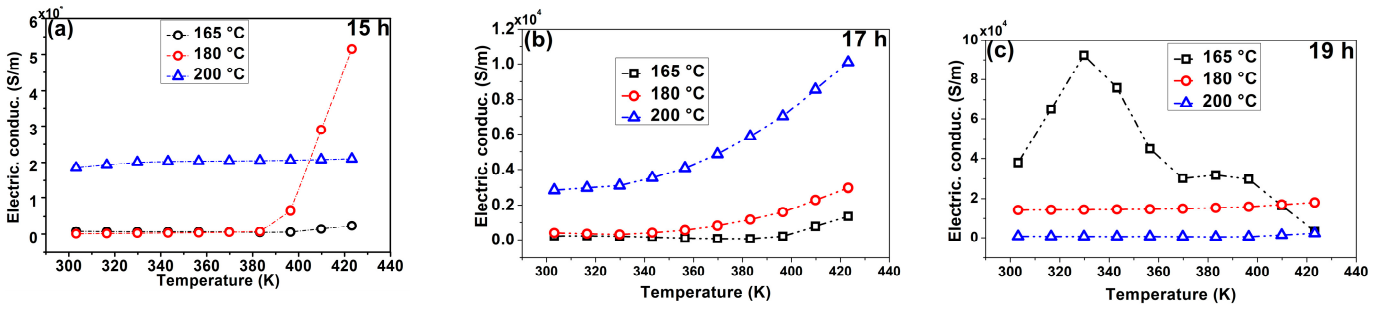

Figure 8. Temperature dependence of electrical conductivity for the samples prepared using the solvothermal method at different processing conditions: (**a**) 15 h, (**b**) 17 h, and (**c**) 19 h. The range of temperature tested was from 303 K to 430 K. (**b**) displays the highest value of electrical conductivity.

3.4.2. Temperature Dependence of Thermal Conductivity

Figure 9 shows the temperature dependence of thermal conductivity. Figure 9a displays the thermal conductivity values of the compounds prepared from 165 °C to 200 °C for 15 h. It can be observed that the compounds produced at 200 °C have the maximum thermal conductivity values, while those produced at 165 °C and 180 °C display thermal conductivity values lower than 0.5 $Wm^{-1}K^{-1}$ in the whole temperature region (363–423 K). The processing temperature may have an impact on the thermal conductivity values of cu-rich tetrahedrites. After 17 h of reaction time (Figure 9b), it was observed that the compounds produced at 200 °C displayed the highest thermal conductivity value (1.08 $Wm^{-1}K^{-1}$) at 423 K. In contrary compounds prepared at 165 °C showed the lowest thermal conductivity (0.65 $Wm^{-1}K^{-1}$) in the whole temperature range analyzed. It is noteworthy that extending the reaction time to 19 h, as depicted in Figure 9c, increased the thermal conductivity (1.04 $Wm^{-1}K^{-1}$ at 423 K) of the compounds prepared at 200 °C, while the compounds prepared at 180 °C exhibited the lowest thermal conductivity values (0.18 $Wm^{-1}K^{-1}$) at

423 K. The compounds produced in this investigation exhibit thermal conductivity values comparable to those reported in other studies [42]. The lower thermal conductivity observed in the compounds generated at 165 °C (15 h and 17 h) could be ascribed to the structural and chemical characteristics of the $Cu_{14}Sb_4S_{13}$ compounds, such as sulfur deficiency-induced carrier defects, impurities, and grain boundary-induced Anderson localization (coupling with other atoms) and the mixture of secondary phases. As seen in the SEM images (Figure 6), many grain boundaries are present, which can significantly reduce the properties of the charge carriers in the Cu-rich compounds, leading to a low thermal conductivity. In the SEM images, micrometer-sized platelets can be observed co-existing with tetrahedrite spheres. In addition, nanostructures are in a hierarchical arrangement to be forming tetrahedrites, which may contribute to the decrease in thermal conductivity. Both electrical and thermal conductivity values, which are critical in determining the TE performance of tetrahedrites, were highly influenced by the reaction time and processing temperature.

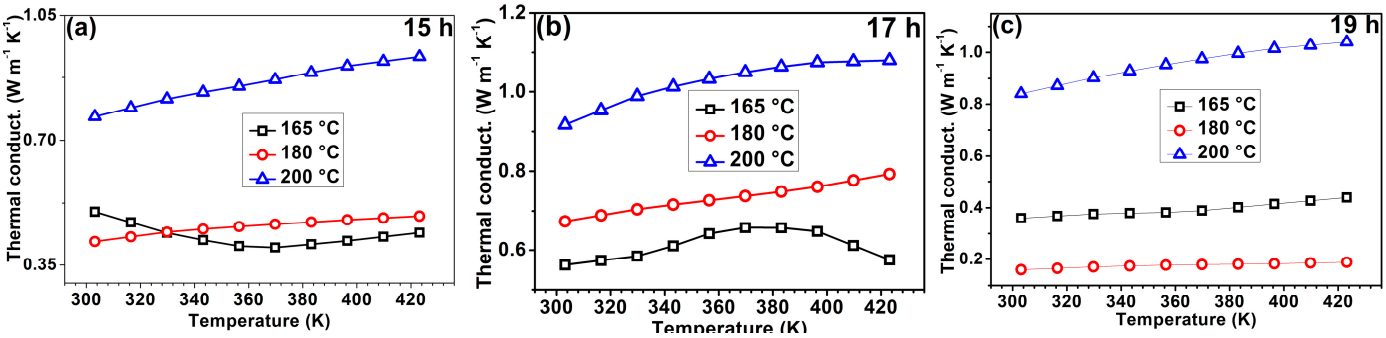

Figure 9. Temperature dependence of thermal conductivity for the samples prepared using the solvothermal method at different processing conditions: (**a**) 15 h, (**b**) 17 h, and (**c**) 19 h. The range of temperature tested was from 303 K to 423 K. The lowest thermal conductivity is achieved by tetrahedrites produced at 165 and 180 °C in the solvothermal process.

Our study suggests that solvothermal parameters, including pressure, temperature, and reaction time, have a significant influence on TE performance of tetrahedrites. The thermal conductivity of tetrahedrites, produced at 200 °C (15 h) and 165 °C (19 h), is significantly reduced from 0.93 Wm^{-1} K^{-1} to 0.439 Wm^{-1} K^{-1} (423 K), respectively. This reduction could lead to the suppression of the bipolar effect, as well as to the substitutional point defect scattering of phonons for further suppression of the effect.

3.4.3. Temperature Dependence of Seebeck Coefficient

Figure 10 depicts the dependence of the Seebeck coefficient. This demonstrates that the synthesis conditions influence the Seebeck coefficient, resulting in both n- and p-type semiconductors. The tetrahedrites fabricated at 200 °C for 15 h were mainly of a p-type. The compounds prepared at 17 h revealed a quite unexpected scenario; as can be seen in Figure 10b, the influence of the preparation temperature is evident. The tetrahedrites fabricated at 165 °C displayed Seebeck coefficient values that suggest that the compounds possess both n- and p-type properties over the entire temperature range studied, demonstrating that, at low temperatures, the preparation of tetrahedrites with thermoelectric performance attributed to a given semiconductor type is complex, possibly due to the occurrence of secondary phases, as shown by the Raman spectra. The Seebeck coefficient value was found to increase with the analysis temperature for compounds prepared at 180 °C. Tetrahedrites synthesized at 17 h and 180 °C yielded a Seebeck coefficient value of 147 μVK^{-1} (423 K). Figure 10c depicts the dependence of the Seebeck coefficient as a function of the temperature range analyzed. The preparation temperature has an influence on the value of the Seebeck coefficient; the compounds obtained at 165 °C show an increase in Seebeck coefficient over the whole temperature range analyzed; it is evident that as

the analysis temperature increases, so does the value of the Seebeck coefficient, whereas the compounds obtained at 180 °C show Seebeck coefficient values very close to zero. At higher preparation temperatures, a slight Seebeck coefficient value is observed. The compounds produced at 200 °C yielded negative Seebeck coefficient values, indicating that n-type tetrahedrite formation is favored at these processing conditions.

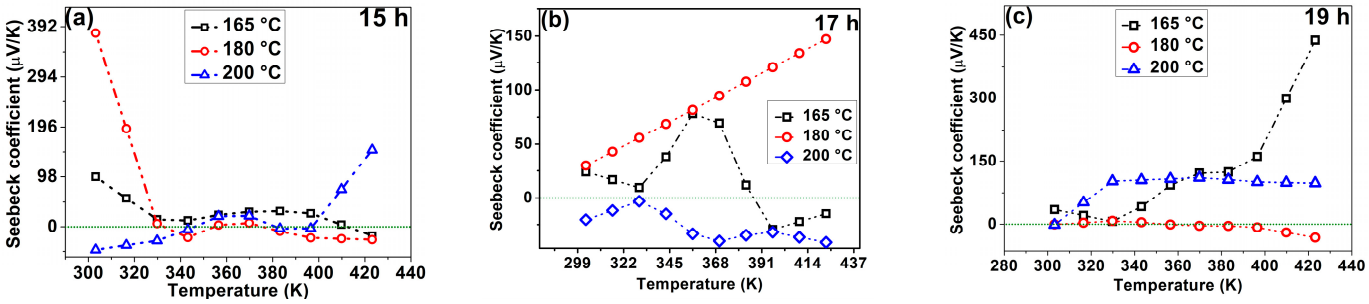

Figure 10. Temperature dependence of Seebeck coefficient for the samples prepared using the solvothermal method at different processing conditions: (**a**) 15 h, (**b**) 17 h, and (**c**) 19 h. The range of temperature tested was from 303 K to 423 K. The highest Seebeck coefficient is achieved in the tetrahedrites produced for 17 h at 180 °C.

The temperature-dependence of the Seebeck coefficient of the tetrahedrites prepared using a reaction time of 19 h is shown in Figure 10c. The tetrahedrites produced at 165 °C exhibited a p-type character throughout the temperature range analyzed. At 423 K, the Seebeck coefficient value was 437 μVK^{-1}. Increasing the processing temperature to 180 °C showed that the tetrahedrites mostly exhibited an n-type nature, as their Seebeck coefficient values were negative in almost the entire temperature range analyzed. At 423 K, the Seebeck coefficient had a value of -32 μVK^{-1}. Our analysis of tetrahedrites prepared at 200 °C revealed that the Seebeck coefficient was predominantly p-type, as evidenced by the positive Seebeck coefficient values. At 423 K, the Seebeck coefficient was 97 μVK^{-1}. The influence of the processing conditions on the Seebeck coefficient of the tetrahedrites produced by the solvothermal method is revealed, and it is shown that such processing conditions can have an influence on the thermoelectric performance. Although the tetrahedrites displayed both p- and n-type semiconductor properties, the highest Seebeck coefficient value at 423 K in the entire range of temperatures analyzed was achieved for tetrahedrites fabricated at 19 h and 165 °C.

The processing conditions allow p-type tetrahedrites to be fabricated by controlling the temperature and reaction time. Figure 11 depicts the temperature dependence of the figure of merit on the preparation parameters. The ZT values of the compounds prepared at 15 h are shown in Figure 11a; ZT values close to zero were achieved for tetrahedrites synthesized at 165 °C, while the highest ZT values were reached for tetrahedrites prepared at 200 °C and 180 °C. Tetrahedrites prepared at 180 °C achieved a ZT equal to 0.3. Figure 11b shows the temperature-dependence of ZT and the influence of the reaction time and processing temperature. It is observed that at the lowest temperature (165 °C), the ZT value is nearly zero. As the temperature increases to 180 °C and 200 °C, the ZT value slightly increases for the compounds prepared at 200 °C, while the ZT value for the tetrahedrites fabricated at 180 °C was 0.35. The processing conditions appear to influence the ZT value, because regardless of the reaction time, the tetrahedrites prepared at 165 °C had a smaller ZT value, whereas the highest ZT value was found in the tetrahedrites prepared at 180 °C. The tetrahedrites prepared at 200 °C had a ZT value of 0.35, whereas the ZT value of the tetrahedrites prepared at 180 °C was 0.35.

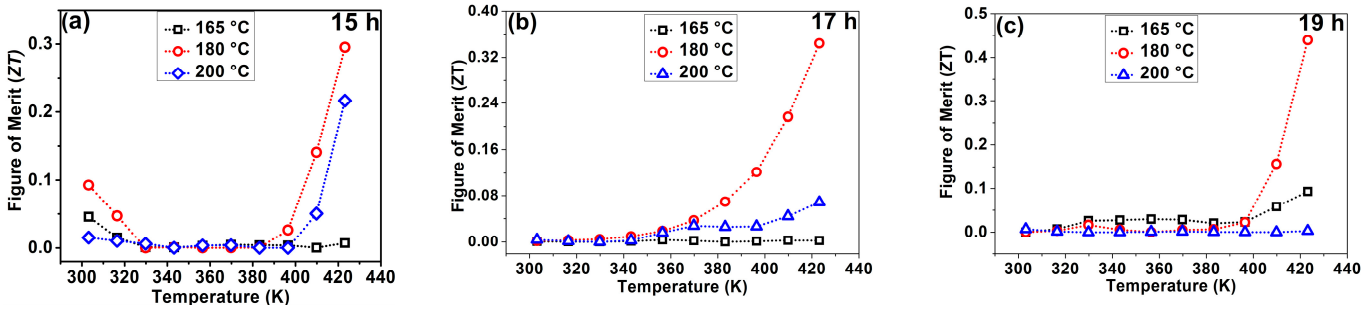

Figure 11. Temperature dependence of ZT of the samples prepared using the solvothermal method at: (**a**) 15 h, (**b**) 17 h, and (**c**) 19 h. The range of temperature tested was from 303 K to 423 K. The highest ZT value is achieved by Cu-rich tetrahedrites produced at 180 °C.

The synthesis parameters significantly influence the thermoelectric properties of tetrahedrites synthesized by the solvothermal method, due to a combination of inherent properties, such as the electrical conductivity, Seebeck coefficient, and thermal conductivity. The unique features of tetrahedrites could be exploited to fabricate materials with the capability to perform thermoelectric power generation. ZT is strongly influenced by the Seebeck coefficient and thermal and electrical conductivity, regardless of the semiconductor material produced in solvothermal processing. In this work, it is demonstrated that although ZT constituents are fundamental for achieving a high figure-of-merit value, the electrical conductivity is crucial for achieving values that are close to the unity. It is interesting to highlight that although the tetrahedrites synthesized at 165 °C and at 15 h appeared to have a lower thermal conductivity than those synthesized at 17 and at 19 h, they do not display a high ZT value, as the electrical conductivity values were relatively small. The Seebeck coefficient values of the compounds prepared from 165 to 200 °C for the 15, 17, and 19 h reaction times are shown in Figure 10a–c. The Seebeck coefficient was measured over the temperature range 303–423 K. Based on the Seebeck coefficient values, by varying the solvothermal processing conditions, both p-type and n-type semiconductors can be produced; nevertheless, the modular values of the Seebeck coefficient are considerably higher for the p-type samples in comparison to the n-type ones. This behavior can be associated with the carrier's concentration and could influence the TE performance. According to results depicted in Figure 10a, the Seebeck coefficients of samples prepared at both 165 °C and 180 °C for 15 h vary over the temperature range (303 K to 423 K). However, the sample prepared at 200 °C showed that the S value increases as the measurement temperature increases. In the mid-temperature range (363 K), the compounds demonstrated p-type conductivity with increasing solvothermal processing temperature. Throughout the entire temperature range (303–423 K), the compounds primarily functioned as p-type semiconductors, suggesting that holes serve as the dominant charge carriers, thus enabling current conduction. When the reaction time increases to 17 h (Figure 10b), we observe that the compounds synthesized at 165 and 180 °C mostly behave as p-type semiconductors in the mid-temperature region (363 K), while the materials produced at 200 °C behave as n-type. An evident trend is observed across the entire temperature range for the compounds produced at 180 °C, although it is evident that both n-type and p-type semiconductors are generated below and after the mid-temperature region, respectively. It is noteworthy that the compounds obtained after 17 h of reaction time at 200 °C, showed predominantly negative Seebeck coefficients and, consequently, are n-type semiconductors, which greatly influence the ZT value.

At 19 h of reaction time, n-type semiconductors are scarce observed in the whole temperature region as the solvothermal processing temperature increases, as shown in Figure 10c. The Seebeck coefficient decreased from 437 to -97 μVK^{-1} (423 K) as the processing temperature increased from 165 °C to 180 °C, respectively. It is important to highlight a dependence of the Seebeck coefficient with both the reaction time and temperature, influencing the thermoelectric performance. This is particularly interesting because of the

relationship between the Seebeck coefficient and ZT. The highest figure-of-merit value could be driven by p-type semiconductors, as evidenced by the Seebeck values obtained over the studied temperature range. Moreover, these compounds exhibited predominantly positive Seebeck coefficients, indicating a p-type thermoelectric performance potentially associated with their structural composition. In this work, we found that p-type semiconductors are responsible for the tetrahedrite-enhanced TE performance. Lee et al. reported on the p-type thermoelectric properties of famatinite Cu_3SbS_4 prepared via mechanical alloying, and they found that both the electrical and thermal conductivity decrease while the Seebeck coefficients increase and ranged from 412 to 670 μVK^{-1} at 323 K and from 482 to 585 μVK^{-1} at 573 K [43]. Goto et al. prepared famatinite, and they reported a Seebeck coefficient of 564 μVK^{-1} at room temperature [44]. On the other hand, Cheng et al. fabricated n-type Mg alloys, and they reported a Seebeck coefficient from −110 to −320 μVK^{-1}, measured in the temperature range of 300–675 K [45].

Famatinite is considered a p-type thermoelectric material which is associated with a positive Seebeck coefficient. According to our Raman and XRD results, the famatinite phase is presented in the Cu-rich compounds produced at 15 and 17 h. The secondary phases could contribute to the significant differences in the Seebeck coefficient values. The variation in the Seebeck values indicates that a p-type or n-type semiconductor has been produced, which has a significant impact in the thermoelectric performance. According to the Seebeck value, a p-type semiconductor was produced at 165 °C. As temperature increases, the Seebeck value seems to randomly influence the thermoelectric performance. The highest values of Seebeck coefficient were yielded for tetrahedrites produced at 180 °C for 17 h.

3.4.4. Temperature Dependence of Figure of Merit, ZT

Figure 11a depicts the ZT measurements of the compounds obtained at 15 h. The materials produced at the lower processing temperature (165 °C) displayed ZT values close to zero over almost the whole measurement temperature range. Increasing the processing temperature to 180 °C also increased the ZT (0.31 at 423 K), while the compounds prepared at 200 °C showed a ZT value of 0.24 at 423 K. The samples synthesized for 17 h yielded significantly different ZT values compared to those obtained after 15 h. Figure 11b shows that while the ZT values for Cu-rich tetrahedrites produced at 165 °C and 200 °C were close to zero for the whole temperature range analyzed, in the mid-temperature range (363 K), the ZT values slightly increased for the compounds produced at 180 °C (0.36 at 423 K). As previously stated in this paper, higher processing temperatures have a significant impact on the fabrication of tetrahedrites and, consequently, on the performance of thermoelectricity. It is worth considering the effect of reaction time, which contributes to the formation of secondary phases that negatively influence the TE properties of the tetrahedrites. ZT values for the compounds prepared over 19 h were measured, and we found that the ZT value increases at lower processing temperatures (165 °C). In contrast, it was observed that the ZT values show small variations above 363 K for synthesis temperatures of 200 °C. The ZT value increases to 0.46 (423 K) for compounds synthesized at 180 °C. The study of Barbier et al. details the production of tetrahedrites and nickel-substituted tetrahedrites to improve TE performance. From their results, it was demonstrated that Ni-doped tetrahedrites achieved a ZT of 0.8 at 700 K due to the combined effects of power factor and thermal conductivity. Different ZT values were observed for samples with similar chemical compositions and comparable preparation methods. Pure tetrahedrites and those doped with Ni, Co, Cr, and Ni have yielded ZT values ranging from 0.6 to 1.2, evaluated at different temperatures, including 600–700 K [46]. However, the highest ZT value obtained in this study significantly increases (after 19 h at 180 °C) in comparison to the values previously reported. A minority of charge carriers, in this case, electrons, are in place at 423 K in the tetrahedrites (180 °C).

The figure of merit measures the TE efficiency and is a very important factor in the conversion of heat to electricity. A high figure of merit is associated with good thermo-

electric materials. From our experiments, we report that the figure of merit of the p-type tetrahedrites is close to 0.5. The preparation method, structural characteristics, and thermoelectric properties of the materials are crucial for a good thermoelectric performance. The processing conditions allow the development of TE properties in materials such as copper-based materials, as they behave as PGEC materials. The TE properties of the materials are determined by several factors, which together optimize the TE efficiency. This opens up new possibilities for the development of high-efficiency TE materials synthesized at low temperatures and reaction times that can help diminish the environmental cost of producing materials for sustainability applications.

3.4.5. Temperature Dependence of Power Factor

The power factor integrates the Seebeck coefficient into the figure of merit. To improve it, it is essential to reduce the thermal conductivity more than the electrical conductivity in the internal interfaces of nanostructures, based on the differences in their respective scattering lengths. The impact of quantum effects on nanostructures has a significant influence on the power factor of the material. Through quantum confinement, the electronic mobility is improved, leading to high electrical conductivity. The PF., which is typically difficult to achieve in bulk materials, can be improved by employing nanoscale materials. An ideal TE material needs to be able to combine low thermal conductivity with a high power factor. Figure 12a shows the PF. Values of the compounds prepared at 15 h. We found that tetrahedrites prepared at lower temperatures (165 and 180 °C) resulted in the lowest values and, consequently, the poorest TE performance when analyzed over the temperature range (303 K–423 K). By increasing the processing temperature to 200 °C, tetrahedrites yielded the highest PF value. This agree with the improved TE values, such as the ZT and Seebeck coefficient.

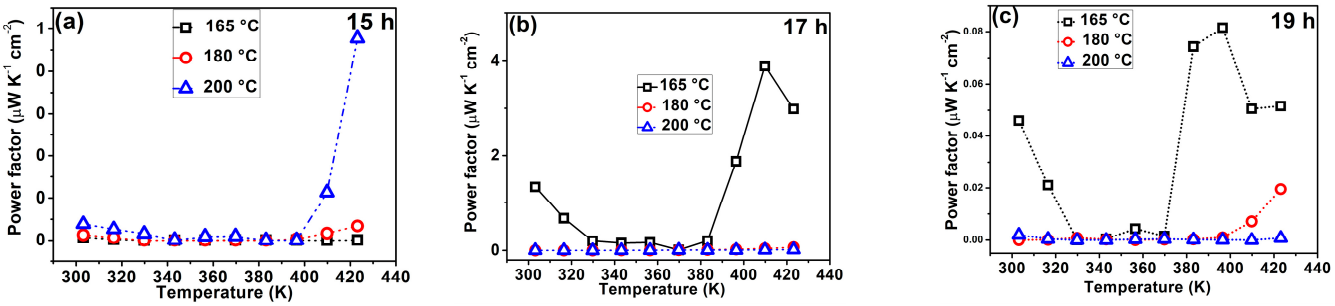

Figure 12. Temperature dependence of power factor for the samples prepared using the solvothermal method at (**a**) 15 h, (**b**) 17 h, and (**c**) 19 h. The range of temperature tested was from 303 K to 430 K. The highest power factor was yielded by Cu-rich tetrahedrites produced during 17 h at 165 °C.

The PF values achieved by the compounds prepared at 17 h (165 180, and 200 °C) are shown in Figure 12b. There is a significant increase in PF in the mid-temperature range (363 K) and then a decrease. Over the temperature range tested (303 K–423 K), most of the PF values remain close to zero. This agrees with the thermal analysis of the samples which were prepared in these conditions. In Figure 12c, the PF values obtained for the tetrahedrites prepared at 19 h are shown. It was observed that this value increases in the mid-temperature region of the analysis (333 K) for those compounds prepared at 200 °C, while for lower processing temperatures (165 and 180 °C), the PF values were lower. It is important to mention that the reaction time has no significant effect on the TE properties of the tetrahedrites, while increasing the processing temperature leads to improved TE performance.

4. Discussion

The thermoelectric mechanism of tetrahedrites can be studied to understand the effect of reducing the thermal conductivity upon increasing the ZT value. The significant

increase in figure of merit and reduction in thermal conductivity are the main contributors to the improved TE properties of the tetrahedrites. The thermoelectric performance of tetrahedrites is directly influenced by the crystalline structure, composition, and synthesis method. Cu-rich tetrahedrites exhibit enhanced Seebeck coefficient values and low thermal conductivity, resulting in an improved ZT value. It has been demonstrated that the solvothermal method is advantageous for the fabrication of tetrahedrites with suitable thermoelectric properties. The influence of solvent is crucial for forming the Cu-rich tetrahedrite phase, since the. solvent provides a medium for the reaction to take place at low temperatures. Ethanol, however, is a polar solvent that can dissolve the precursors. Due to its low viscosity, it facilitates better mixing of the reactants, promoting uniform nucleation and growth of the tetrahedrites. The appropriate selection of the solvent medium is crucial for the morphology and phase of the products. It is possible to successfully control the reaction process by choosing the appropriate reaction media, as well as the reaction temperature. There are important factors that influence the phase purity of the products, which have important implications for the solvothermal method. These factors may provide a general route for the selective preparation of other semiconducting sulfide nanocrystallites. Due to the nanostructuring and grain boundaries that contribute to the improvement of thermoelectric performance, the solvothermal method is suitable to produce materials with low thermal conductivity. In the future, it will be essential to develop innovative materials that focus on environmentally friendly manufacturing with potential applications in thermoelectric materials research. The influence of the solvent, reaction time, and temperature plays a crucial role in achieving a cubic-phase tetrahedrite with a good thermoelectric performance. Furthermore, it is responsible for electronic structure, charge carrier density, mobility, and thermal conductivity properties. As previously discussed in this article, the rattling phenomenon in the crystal lattice is primarily attributable to the crystal structure of tetrahedrites. This allows copper ions to move in defined boxes, disrupting phonon propagation, resulting in a decrease in thermal conductivity, which in turn could explain the thermal properties of the Cu-rich tetrahedrites reported. The PF values yielded in this investigation are in good agreement with those values reported in other studies. Yan et al. reported average PF values of representative polycrystalline TE materials within their measured temperature ranges [47]. Yan et al. also reported a maximum ZT of 1.1 for tetrahedrites when the electrical and thermal transports were properly balanced, with a PF of 1.2 $mWm^{-1}K^{-2}$ at 723 K [48]. Mn-doped tetrahedrites exhibited a high ZT of 1.1 at a power factor of 0.5 $mWm^{-1}K^{-2}$ at 573 K [49]. Wet chemically synthesized Zn-doped tetrahedrites have demonstrated a high ZT of 1.1 with a limited PF value of less than 0.5 $mWm^{-1}K^{-2}$, making them far from fit for practical use. To achieve an improved TE performance, it is therefore necessary to reduce thermal conductivity and to increase the PF, which is responsible for the ZT value at high temperatures [47]. ZT combines the Seebeck coefficient, electrical conductivity, and thermal conductivity, $(ZT = \frac{S^2\sigma T}{k})$, and these parameters are generally responsible for the thermoelectric efficiency. A high PF and a low thermal conductivity are required for achieving a high ZT, according to the formula. Although the power factor $(P.F. = S^2\sigma)$ is a significant contributing factor to ZT, it is not the only factor. If the thermal conductivity of a material is high, it can possess a high PF while still exhibiting a low ZT. Therefore, understanding ZT allows us to identify and optimize the interaction between the parameters to improve the overall thermoelectric performance. By focusing on ZT, we can find materials with a high power factor and good thermal properties. For instance, materials such as Cu-rich tetrahedrites have been reported to have good ZT values, indicating their potential for practical applications. It is important to consider the role of ZT in a comprehensive evaluation of the efficiency of thermoelectric materials, not only the power factor value. This will facilitate the optimization of their performance for future practical applications. From our results, we see that tetrahedrite synthesized at 180 °C for 19 h resulted in an improved ZT of 0.46 and a thermal conductivity of 0.2 $Wm^{-1}\ K^{-1}$ (423 K). The unwanted contribution of thermal conductivity also reduces the Seebeck coefficient, thus limiting the ZT values at higher temperatures. This results in a

detrimental effect on the TE performance, possibly related to the reduction in Sb^{5+} species. Increasing the processing temperature to 165 °C leads to a decrease in the Sb^{3+}/Sb^{5+} ratio and an increase in the Cu^{+}/Cu^{2+} ratio due to the transformation of the secondary phases into the tetrahedrite phase. From the XPS results, the maximum amount of Sb^{5+} species is detected in samples synthesized for 19 h at 165 °C, while the minimum amount is observed in the samples produced for 15 h at 200 °C. The results show agreement with the Seebeck coefficient, figure of merit, and power factor values. This assumption seems reasonable since the power factor is related to the Seebeck coefficient. We can therefore conclude that the antimony species are responsible for promoting valuable thermoelectric performance.

5. Conclusions

In summary, we describe the production of copper-based materials via the solvothermal method. This investigation demonstrated that structural changes occur at moderately low temperatures (165 °C) and that increasing the temperature to 200 °C yields a purer phase of tetrahedrites. Maximum ZT values of 0.46 can be achieved at 423 K for tetrahedrites synthesized at 19 h (180 °C). The results demonstrated that both the processing time and temperature are crucial in controlling the phase and morphology of the final products. Both p-type and n-type semiconductors were produced by varying both the reaction time and temperature; nevertheless, the modular values of the Seebeck coefficient are considerably higher for the p-type samples in comparison to the n-type ones. The solvothermal method can be employed to fabricate ternary semiconductors with a high thermoelectric performance.

Supplementary Materials: The following supporting information can be downloaded at https://www.mdpi.com/article/10.3390/cryst14100888/s1, Figure S1: Schematic representation of the process carried out for synthesizing Cu-rich tetrahedrites; Figure S2: FTIR spectra ranged from 650 to 750 cm^{-1}: Figure S3: Raman spectra of the vibrational mode at 352 cm^{-1} attributed to the tetrahedrite phase; Figure S4: Sb core-level of the compounds prepared at 15, 17, and 19 h; cell parameter; Figure S5: Sb^{3+}/Sb^{5+} ratio of the compounds prepared at different solvothermal conditions; Figure S6: cell parameters of the compounds prepared with different processing conditions, such as time and temperature; Figure S7: SEM micrographs and XEDS of Cu-rich tetrahedrites; Figure S8: TEM micrographs and SAED pattern of tetrahedrites; Table S1: Chi-square value extracted from the XPS data.

Author Contributions: Conceptualization, E.R.G. and A.B.L.-O.; methodology, I.J.S.-C.; validation, E.R.G., A.B.L.-O., M.A.A.-F. and D.D.Á.-L.; formal analysis, E.R.G. and A.B.L.-O.; investigation, I.J.S.-C.; resources, E.R.G.; data curation, I.J.S.-C. and J.J.R.-V.; writing—original draft preparation, I.J.S.-C.; writing—review and editing, E.R.G., D.D.Á.-L. and A.B.L.-O.; visualization, E.R.G., D.D.Á.-L. and A.B.L.-O.; supervision, E.R.G., D.D.Á.-L. and A.B.L.-O.; project administration, E.R.G.; funding acquisition, E.R.G. All authors have read and agreed to the published version of the manuscript.

Funding: This research was funded by Conahcyt (Projects 315884; 042), SIP IPN (Projects 20220655, 20230826, 20240595, 20242786, and 20240290), and the APC, as was funded by Instituto Politécnico Nacional.

Data Availability Statement: The original contributions presented in this study are included in the article/Supplementary Material, further inquiries can be directed to the corresponding authors.

Acknowledgments: Soní-Castro is grateful for her postgraduate fellowship to Conahcyt. The authors express their gratitude to Conahcyt for the financial support received through projects 315884, 042, and SNII-Conahcyt and to CNMN-IPN for XPS, Raman spectroscopy, and TEM characterizations. The authors express their gratitude to Percival Soní-Castro for SEM images and Sebastian Pacheco for XRD measurements.

Conflicts of Interest: The authors declare no conflicts of interest.

References

1. Fernandes, L.; Fernández, E.; Martins, P.; Ferreira, N.; Antunes, P.; Lanceros-Mendez, S. Overview on thermoactive materials, simulations and applications. *J. Mater. Sci.* **2020**, *55*, 925–946. [CrossRef]

2. Mehdizadeh Dehkordi, A.; Zebarjadi, M.; He, J.; Tritt, T.M. Thermoelectric power factor: Enhancement mechanisms and strategies for higher performance thermoelectric materials. *Mater. Sci. Eng. R Rep.* **2015**, *97*, 1–22. [CrossRef]
3. Bhattacharya, S.; Basu, R.; Bhatt, R.; Pitale, S.; Singh, A.; Aswal, D.K.; Gupta, S.K.; Navaneethan, M.; Hayakawa, Y. $CuCrSe_2$: A high performance phonon glass and electron crystal thermoelectric material. *J. Mater. Chem. A* **2013**, *1*, 11289–11294. [CrossRef]
4. Qian, X.; Zhou, J.; Chen, G. Phonon-engineered extreme thermal conductivity materials. *Nat. Mater.* **2021**, *20*, 1188–1202. [CrossRef]
5. Beekman, M.; Morelli, D.T.; Nolas, G.S. Better thermoelectrics through glass-like crystals. *Nat. Mater.* **2015**, *14*, 1182–1185. [CrossRef]
6. Renthlei, Z.; Celestine, L.; Kima, L.; Zuala, L.; Mawia, Z.; Chettri, B.; Singh, Y.T.; Abdullaev, S.; Ezzeldien, M.; Rai, D.P. Theoretical Investigation of Lead Perovskite $PbXO_3$ (X = Ti, Zr, and Hf) for Potential Thermoelectric Applications: Hybrid-DFT Approach. *Energy Fuels* **2023**, *37*, 19831–19844. [CrossRef]
7. Li, B.; Li, M.; Qi, H.; Zu, X.; Qiao, L.; Xiao, H. The Effects of Chlorine Doping on the Thermoelectric Properties of Bi_2O_2Se. *Crystals* **2023**, *13*, 1586. [CrossRef]
8. Behera, D.; Akila, B.; Amraoui, R.; Kadri, S.; Mukherjee, S.K.; Salah, M.M.; Saeed, A. Excellent Thermoelectric Performance in KBaTh (Th = Sb, Bi) Based Half-Heusler Compounds and Design of Actuator for Efficient and Sustainable Energy Harvesting Applications. *Crystals* **2023**, *13*, 1551. [CrossRef]
9. Wang, W.; Xian, C.; Ou, Y.; He, Z.; Xie, S. Thermoelectric Properties of PbS Doped with Bi_2S_3 and Cu_2S Prepared by Hydrothermal Synthesis and Spark Plasma Sintering. *Crystals* **2023**, *13*, 764. [CrossRef]
10. Wuensch, B.J. The crystal structure of tetrahedrite, $Cu1_2Sb_4S_{18}$. *Z. Für Krist.-Cryst. Mater.* **1964**, *119*, 437–453. [CrossRef]
11. Lu, X.; Morelli, D.T. Rapid synthesis of high-performance thermoelectric materials directly from natural mineral tetrahedrite. *MRS Commun.* **2013**, *3*, 129–133. [CrossRef]
12. Lai, W.; Wang, Y.; Morelli, D.T.; Lu, X. From Bonding Asymmetry to Anharmonic Rattling in Cu12Sb4S13 Tetrahedrites: When Lone-Pair Electrons Are Not So Lonely. *Adv. Funct. Mater.* **2015**, *25*, 3648–3657. [CrossRef]
13. Zazakowny, K.; Kosonowski, A.; Lis, A.; Cherniushok, O.; Parashchuk, T.; Tobola, J.; Wojciechowski, K.T. Phase Analysis and Thermoelectric Properties of Cu-Rich Tetrahedrite Prepared by Solvothermal Synthesis. *Materials* **2022**, *15*, 849. [CrossRef] [PubMed]
14. Lee, G.-E.; Kim, I.-H. Skinnerite Cu_3SbS_3: Solid-State Synthesis and Thermoelectric Properties. *Korean J. Met. Mater.* **2022**, *60*, 455–462. [CrossRef]
15. Baláž, P.; Guilmeau, E.; Daneu, N.; Dobrozhan, O.; Baláž, M.; Hegedus, M.; Barbier, T.; Achimovičová, M.; Kaňuchová, M.; Briančin, J. Tetrahedrites Synthesized via Scalable Mechanochemical Process and Spark Plasma Sintering. *J. Eur. Ceram. Soc.* **2020**, *40*, 1922–1930. [CrossRef]
16. Kareem, M.Q.; Ameen, M.M.; Hassan, S.A.; Shareef, S.M. Synthesis of Tetrahedrite Zincian Nanocomposites via solvothermal process at low temperature. *Ceram. Int.* **2024**, *50*, 40005–40013. [CrossRef]
17. Demazeau, G. Solvothermal Processes: Definition, Key Factors Governing the Involved Chemical Reactions and New Trends. *Z. Für Naturforschung B* **2010**, *65*, 999–1006. [CrossRef]
18. Ni, X.; Zhang, J.; Zhao, L.; Wang, F.; He, H.; Dramou, P. Study of the solvothermal method time variation effects on magnetic iron oxide nanoparticles (Fe_3O_4) features. *J. Phys. Chem. Solids* **2022**, *169*, 110855. [CrossRef]
19. An, C.; Jin, Y.; Tang, K.; Qian, Y. Selective synthesis and characterization of famatinite nanofibers and tetrahedrite nanoflakes. *J. Mater. Chem.* **2003**, *13*, 301–303. [CrossRef]
20. Lis, A.; Zazakowny, K.; Cherniushok, O.; Tobola, J.; Gajewska, M.; Parashchuk, T.; Wojciechowski, K.T. Nanostructured Cu_{12} + xSb_4S_{13} tetrahedrites prepared by solvothermal synthesis in 1-(2-aminoethyl)piperazine for efficient thermal energy harvesting. *J. Alloys Compd.* **2024**, *977*, 173337. [CrossRef]
21. James, D.J.; Lu, X.; Morelli, D.T.; Brock, S.L. Solvothermal Synthesis of Tetrahedrite: Speeding up the Process of Thermoelectric Material Generation. *ACS Appl. Mater. Interfaces* **2015**, *7*, 23623–23632. [CrossRef] [PubMed]
22. Khan, I.; Saeed, K.; Khan, I. Nanoparticles: Properties, applications and toxicities. *Arab. J. Chem.* **2019**, *12*, 908–931. [CrossRef]
23. Alqahtani, T.; Khan, M.D.; Lewis, D.J.; Zhong, X.L.; O'Brien, P. Scalable synthesis of Cu–Sb–S phases from reactive melts of metal xanthates and effect of cationic manipulation on structural and optical properties. *Sci. Rep.* **2021**, *11*, 1887. [CrossRef]
24. Rath, T.; MacLachlan, A.J.; Brown, M.D.; Haque, S.A. Structural, optical and charge generation properties of chalcostibite and tetrahedrite copper antimony sulfide thin films prepared from metal xanthates. *J. Mater. Chem. A* **2015**, *3*, 24155–24162. [CrossRef] [PubMed]
25. Prem Kumar, D.S.; Ren, M.; Osipowicz, T.; Mallik, R.C.; Malar, P. Tetrahedrite ($Cu_{12}Sb_4S_{13}$) thin films for photovoltaic and thermoelectric applications. *Sol. Energy* **2018**, *174*, 422–430. [CrossRef]
26. Pattrick, R.A.D.; van der Laan, G.; Vaughan, D.J.; Henderson, C.M.B. Oxidation state and electronic configuration determination of copper in tetrahedrite group minerals by L-edge X-ray absorption spectroscopy. *Phys. Chem. Miner.* **1993**, *20*, 395–401. [CrossRef]
27. Rossi, A.; Atzei, D.; Da Pelo, S.; Frau, F.; Lattanzi, P.; England, K.E.R.; Vaughan, D.J. Quantitative X-ray photoelectron spectroscopy study of enargite (Cu_3AsS_4) surface. *Surf. Interface Anal.* **2001**, *31*, 465–470. [CrossRef]
28. Wang, L.; Yang, B.; Xia, Z.; Leng, M.; Zhou, Y.; Xue, D.-J.; Zhong, J.; Gao, L.; Song, H.; Tang, J. Synthesis and characterization of hydrazine solution processed $Cu_{12}Sb_4S_{13}$ film. *Sol. Energy Mater. Sol. Cells* **2016**, *144*, 33–39. [CrossRef]

29. Medina-Montes, M.I.; Campos-González, E.; Morales-Luna, M.; Sánchez, T.G.; Becerril-Silva, M.; Mayén-Hernández, S.A.; de Moure-Flores, F.; Santos-Cruz, J. Development of phase-pure $CuSbS_2$ thin films by annealing thermally evaporated CuS/Sb_2S_3 stacking layer for solar cell applications. *Mater. Sci. Semicond. Process.* **2018**, *80*, 74–84. [CrossRef]
30. Amri, A.; Duan, X.; Yin, C.-Y.; Jiang, Z.-T.; Rahman, M.M.; Pryor, T. Solar absorptance of copper–cobalt oxide thin film coatings with nano-size, grain-like morphology: Optimization and synchrotron radiation XPS studies. *Appl. Surf. Sci.* **2013**, *275*, 127–135. [CrossRef]
31. Karikalan, N.; Karthik, R.; Chen, S.-M.; Karuppiah, C.; Elangovan, A. Sonochemical Synthesis of Sulfur Doped Reduced Graphene Oxide Supported CuS Nanoparticles for the Non-Enzymatic Glucose Sensor Applications. *Sci. Rep.* **2017**, *7*, 2494. [CrossRef] [PubMed]
32. Gurgul, J.; Rinke, M.T.; Schellenberg, I.; Pöttgen, R. The antimonide oxides REZnSbO and REMnSbO (RE = Ce, Pr)—An XPS study. *Solid State Sci.* **2013**, *17*, 122–127. [CrossRef]
33. Vinayakumar, V.; Shaji, S.; Avellaneda, D.; Das Roy, T.K.; Castillo, G.A.; Martinez, J.A.A.; Krishnan, B. $CuSbS_2$ thin films by rapid thermal processing of Sb_2S_3-Cu stack layers for photovoltaic application. *Sol. Energy Mater. Sol. Cells* **2017**, *164*, 19–27. [CrossRef]
34. Wan, L.; Guo, X.; Fang, Y.; Mao, X.; Guo, H.; Xu, J.; Zhou, R. Spray pyrolysis deposited CuSbS2 absorber layers for thin-film solar cells. *J. Mater. Sci. Mater. Electron.* **2019**, *30*, 21485–21494. [CrossRef]
35. Lv, H.; Qiu, S.; Lu, G.; Fu, Y.; Li, X.; Hu, C.; Liu, J. Nanostructured Antimony/carbon Composite Fibers as Anode Material for Lithium-ion Battery. *Electrochim. Acta* **2015**, *151*, 214–221. [CrossRef]
36. Bincy, J. Temperature dependent solvothermal synthesis of Cu-Sb-S nanoparticles with tunable structural and optical properties. *Mater. Res. Bull.* **2017**, *95*, 267–276. [CrossRef]
37. An, C.; Liu, Q.; Tang, K.; Yang, Q.; Chen, X.; Liu, J.; Qian, Y. The influences of surfactant concentration on the quality of chalcostibite nanorods. *J. Cryst. Growth* **2003**, *256*, 128–133. [CrossRef]
38. Fasolin, S.; Fiameni, S.; Fanciulli, C.; Battiston, S.; Famengo, A.; Fabrizio, M. Nanostructured Tetrahedrite Synthesis for Thermoelectric Applications. *J. Nanosci. Nanotechnol.* **2017**, *17*, 1645–1649. [CrossRef]
39. Wang, Q.; Li, J.; Li, J. Enhanced thermoelectric performance of Cu_3SbS_4 flower-like hierarchical architectures composed of Cl doped nanoflakes via an in situ generated CuS template. *Phys. Chem. Chem. Phys.* **2018**, *20*, 1460–1475. [CrossRef]
40. Regulacio, M.D.; Tee, S.Y.; Lim, S.H.; Teng, C.P.; Koh, L.-D.; Liu, S.; Han, M.-Y. Facile solvothermal approach to pristine tetrahedrite nanostructures with unique multiply-voided morphology. *Nanoscale* **2017**, *9*, 17865–17876. [CrossRef]
41. Sun, F.-H.; Dong, J.; Tang, H.; Shang, P.-P.; Zhuang, H.-L.; Hu, H.; Wu, C.-F.; Pan, Y.; Li, J.-F. Enhanced performance of thermoelectric nanocomposites based on Cu12Sb4S13 tetrahedrite. *Nano Energy* **2019**, *57*, 835–841. [CrossRef]
42. López Cota, F.A.; Díaz-Guillén, J.A.; Juan Dura, O.; López de la Torre, M.A.; Rodríguez-Hernández, J.; Fernández Fuentes, A. Mechanosynthesis and Thermoelectric Properties of Fe, Zn, and Cd-Doped P-Type Tetrahedrite: Cu_{12}-xMxSb_4S_{13}. *Materials* **2021**, *14*, 3448. [CrossRef] [PubMed]
43. Lee, G.-E.; Pi, J.-H.; Kim, I.-H. Preparation and Thermoelectric Properties of Famatinite Cu_3SbS_4. *J. Electron. Mater.* **2020**, *49*, 2781–2788. [CrossRef]
44. Goto, Y.; Sakai, Y.; Kamihara, Y.; Matoba, M. Effect of Sn-Substitution on Thermoelectric Properties of Copper-Based Sulfide, Famatinite Cu_3SbS_4. *J. Phys. Soc. Jpn.* **2015**, *84*, 044706. [CrossRef]
45. Cheng, K.; Bu, Z.; Tang, J.; Zhang, X.; Meng, X.; Li, W.; Pei, Y. Efficient $Mg_2Si_{0.3}Sn_{0.7}$ thermoelectrics demonstrated for recovering heat of about 600 K. *Mater. Today Phys.* **2022**, *28*, 100887. [CrossRef]
46. Barbier, T.; Lemoine, P.; Gascoin, S.; Lebedev, O.I.; Kaltzoglou, A.; Vaqueiro, P.; Powell, A.V.; Smith, R.I.; Guilmeau, E. Structural stability of the synthetic thermoelectric ternary and nickel-substituted tetrahedrite phases. *J. Alloys Compd.* **2015**, *634*, 253–262. [CrossRef]
47. Yan, Y.; Li, N.; Wang, G.; Xiong, Q.; Fan, L.; Jiang, P.; Lu, X.; Wang, G.; Zhou, X. Achieving high average power factor in tetrahedrite $Cu_{12}Sb_4S_{13}$ via regulating electron-phonon coupling strength. *Mater. Today Phys.* **2022**, *22*, 100590. [CrossRef]
48. Yan, Y.; Wu, H.; Wang, G.; Lu, X.; Zhou, X. High thermoelectric performance balanced by electrical and thermal transport in tetrahedrites Cu_{12}+xSb_4S_{12}Se. *Energy Storage Mater.* **2018**, *13*, 127–133. [CrossRef]
49. Chetty, R.; DS, P.K.; Rogl, G.; Rogl, P.; Bauer, E.; Michor, H.; Suwas, S.; Puchegger, S.; Giester, G.; Mallik, R.C. Thermoelectric properties of a Mn substituted synthetic tetrahedrite. *Phys. Chem. Chem. Phys.* **2015**, *17*, 1716–1727. [CrossRef]